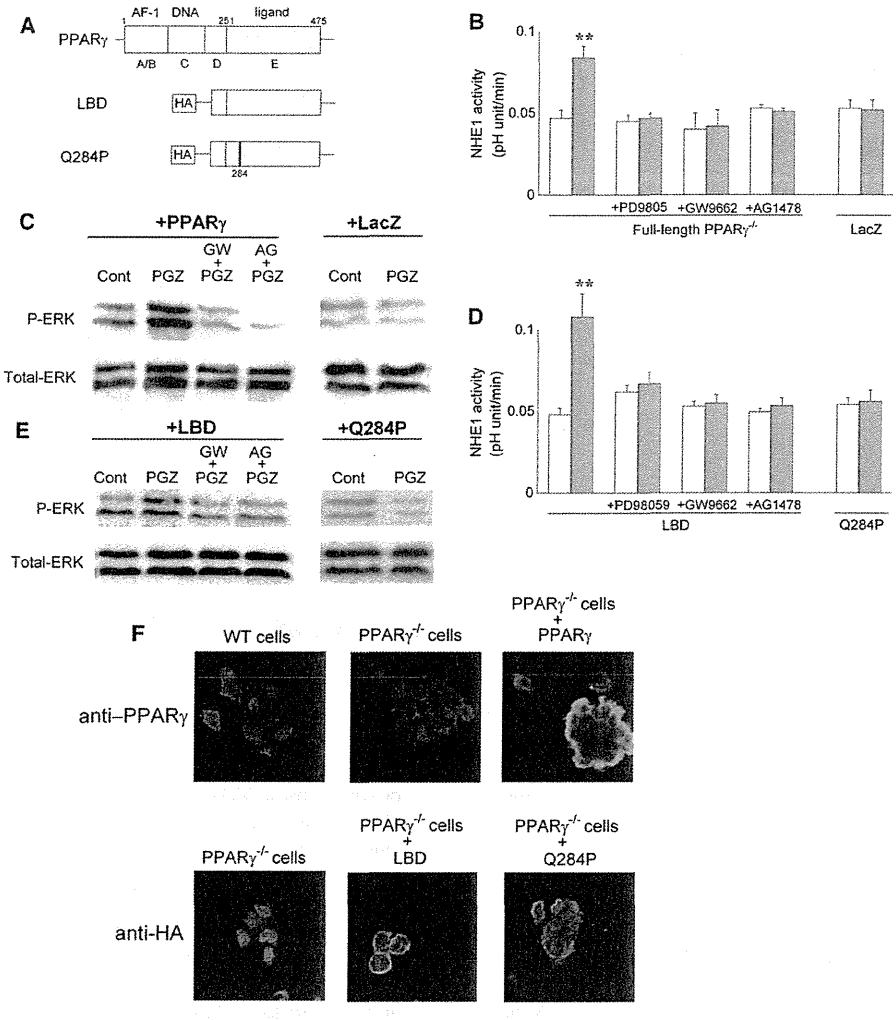

Figure 6. Effects of Adenovirus-Mediated Transfer of PPARγ Constructs into PPARγ$^{-/-}$ Cells

(A) PPARγ constructs. AF-1, transcription activation function domain; DNA, DNA-binding domain; ligand, ligand-binding domain; HA, hemagglutinin.

(B) Full-length PPARγ rescued the PGZ-mediated stimulation of NHE1 activity. Open bars represent the control activities and closed bars represent the activities in the presence of 0.3 μM PGZ. **$p < 0.01$ versus control. Data are means ± SEM of six to seven experiments.

(C) Full-length PPARγ, but not LacZ, rescued the PGZ-mediated ERK phosphorylation.

(D) LBD, but not Q284P, rescued the PGZ-mediated stimulation of NHE1 activity. Open bars represent the control activities and closed bars represent the activities in the presence of 0.3 μM PGZ. **$p < 0.01$ versus control. Data are means ± SEM of six to seven experiments.

(E) LBD, but not Q284P, rescued the PGZ-mediated ERK phosphorylation.

(F) Expression of endogenous PPARγ or PPARγ constructs in EF cells. Immunohistochemical analysis was performed by using the anti-PPARγ antibody or the anti-HA antibody. Green shows PPARγ or LBD constructs, red shows actin, and blue shows nuclei. See also Figure S5.

In addition, the chronic administration of TZDs in rats was reported to enhance the renal abundance of α1 subunit of Na^+/K^+ ATPase and the apical Na^+/H^+ exchanger NHE3 in PTs (Song et al., 2004). TZDs were also found to enhance the expression of NHE3 through SGK1-mediated transcriptional activity of PPARγ in cultured human PT cells (Saad et al., 2009). These changes in transporter abundance may further amplify the TZD-induced nongenomic stimulation of PT transport in species other than mice. Consistent with this view, the reduction in lithium clearance was indeed reported in human subjects treated with TZDs (Zanchi et al., 2004). Diuretics targeting the distal nephrons were at least partially effective in preventing TZD-induced mild volume expansion in human subjects with type 2 diabetes (Karalliedde et al., 2006). However, massive volume expansion, the clinically more important side effect sometimes observed in human subjects taking TZDs, is known to be resistant to the conventional diuretic monotherapy (Mudaliar et al., 2003). These considerations support a view that a mechanism other than the stimulation of distal nephron transport is also involved in TZD-induced fluid retention in humans.

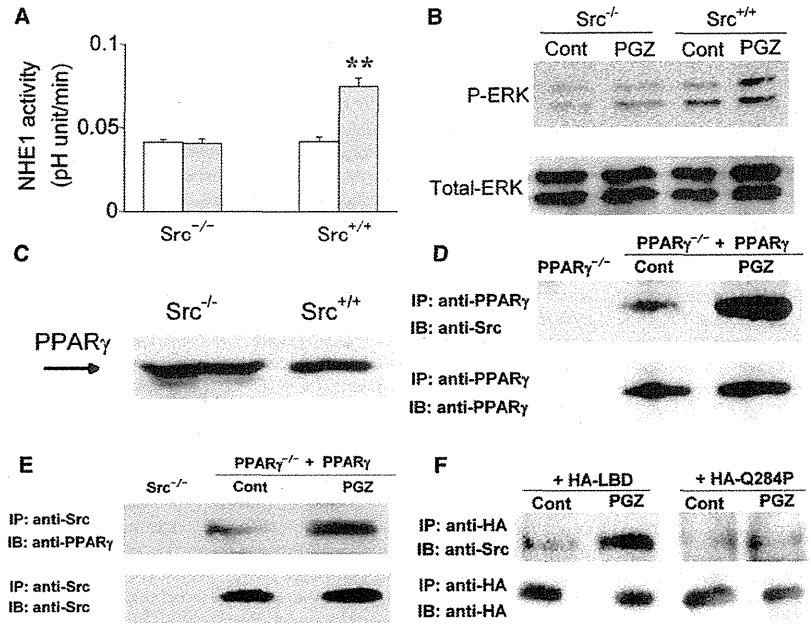

Figure 7. Roles of Src in TZD-Induced Rapid Signaling in EF Cells

(A) Effects of PGZ on NHE1 activity in $Src^{-/-}$ and $Src^{+/+}$ cells. Open bars represent the control activities and closed bars represent the activities in the presence of 0.3 μM PGZ. $^{**}p < 0.01$ versus control. Data are means ± SEM. Each n = 6.

(B) PGZ stimulated ERK phosphorylation in $Src^{+/+}$ cells, but not in $Src^{-/-}$ cells. PGZ (0.3 μM) was added for 5 min.

(C) Western blot analysis was performed by using the anti-PPARγ antibody in $Src^{-/-}$ and $Src^{+/+}$ cells.

(D) Immunoprecipitation with the anti-PPARγ antibody in $PPAR\gamma^{-/-}$ cells without or with PPARγ transfection.

(E) Immunoprecipitation with the anti-Src antibody in $Src^{-/-}$ cells (left) or $PPAR\gamma^{-/-}$ cells transfected with PPARγ (middle and right). PGZ (0.3 μM) was added for 5 min.

(F) Immunoprecipitation with the anti-HA antibody in $PPAR\gamma^{-/-}$ cells transfected with LBD or Q284P. PGZ (0.3 μM) was added for 5 min.

In this context, it is noteworthy that the stimulation of sodium transport in distal nephrons alone, induced by excessive aldosterone actions, usually does not result in massive volume expansion with edema formation, because a process known as the "escape phenomenon" suppresses the sodium reabsorption along PTs and other nephron segments (Gonzalez-Campoy et al., 1989). On the other hand, the simultaneous stimulation of sodium transport in PTs and distal nephrons through distinct mechanisms is expected, at least under certain conditions, to operate in a synergic manner. Massive volume expansion in human subjects usually occurs after weeks of use of TZDs. However, it can also occur as rapidly as 4 days after use of TZDs (Hirsch et al., 1999), supporting the involvement of multiple mechanisms. Thus, combination therapy with different diuretics targeting both PTs and the distal nephrons could be a therapeutic option in case of TZD-induced massive volume expansion.

Finally, this study represents an alternative paradigm in the emerging concept that nuclear hormone receptors can mediate nongenomic actions (Lösel and Wehling, 2003). Different ligands can bind to LBD of PPARγ in slightly different ways and induce different biological responses (Zhang et al., 2007). It could be possible, therefore, to discriminate the diverse PPARγ actions at least partially by modifying the ligand-induced conformational changes. Indeed, several selective PPARγ modulators developed by such a concept are known to induce less fluid retention at least in animals (Higgins and Depaoli, 2010). Future studies are required to determine whether these selective PPARγ modulators can also prevent massive fluid retention in humans.

EXPERIMENTAL PROCEDURES

Measurements of NBCe1 and NHE3 Activities in Renal Proximal Tubules

All animal procedures were in accordance with local institutional guidelines. Japanese white rabbits, Wistar rats, or C57BL/6 mice were sacrificed with excessive amounts of pentobarbital and thin slices of kidney cortex were obtained. For human PTs, kidney cortex tissues were obtained during the unilateral nephrectomy for renal carcinoma. The institutional review board of University of Tokyo School of Medicine approved the study and written informed consent was obtained from all the subjects. The PT (S2 segment) fragment was microdissected manually and transferred to a perfusion chamber mounted on an inverted microscope. For the analysis of NBCe1 activity, the luminally collapsed tubule was used as described (Li et al., 2008). The tubule was incubated with an acetoxymethyl ester form of a pH-sensitive fluorescence dye 2′,7′-bis(carboxyethyl)-5(6)-carboxyfluorescein (BCECF/AM; Dojindo) and pH_i was monitored with a photometry system (OSP-10; Olympus). Calibration curves for pH_i were obtained according to the method described (Thomas et al., 1979). Prewarmed (38°C) Dulbecco's modified Eagle's medium (DMEM) equilibrated with 5% CO_2/95% O_2 gas was used for the peritubular perfusate, which was shown to be essential for the long-term functional preservation of isolated PTs (Müller-Berger et al., 1997; Zheng et al., 2003) The rate of pH_i decrease to bath HCO_3^- reduction and the buffer capacity were used to calculate the NBCe1 activity as described (Li et al., 2008). For the analysis of NHE3 activity, pH_i was monitored in the microperfused S2 segment as described (Yamada et al., 1996). Initially, both luminal and bath sides were perfused with HEPES-buffered Ringer solution equilibrated with 100% O_2 and thereafter, luminal perfusate was switched to Na^+-free HEPES solution that replaces Na^+ in HEPES-buffered Ringer solution with N-methyl-D-glucamine. The resultant decrease in pH_i was shown to reflect the luminal NHE3 activity (Yamada et al., 1996).

Determination of Bicarbonate Absorption Rates

We used the stop-flow microspectrofluorometric method as described (Müller-Berger et al., 1999; Zheng et al., 2003). Isolated PTs were microperfused and luminal pH (pH_L) was monitored on the OSP-10 system. The tubular lumen was perfused with Ringer solution, which contained 25 mM HCO_3^-, 40 mM raffinose, and 40 mM BCECF, and DMEM was used for the bath perfusate. To determine $JHCO_3^-$, we abruptly stopped the rapid (~80 nl/min) luminal perfusion by suddenly reducing the perfusion pressure from ~18 to 0 cm H_2O. The decay in luminal HCO_3^- concentration was calculated from the changes in pH_L and $JHCO_3^-$ was calculated as described (Müller-Berger et al., 1999).

Renal Clearance Protocol

Adult female Wistar rats weighing between 140 and 170 g were used. The rats were individually housed in metabolic cages. Three days before study, the diet

was changed from a standard diet to one containing lithium chloride (6 mM/kg dry weight) to yield measurable plasma lithium concentrations without affecting renal function (Shalmi and Thomsen, 1989). On the morning of clearance study water and food were withdrawn and maximal diuresis was induced by water loading to facilitate the detection of rapid alterations in PT transport. Each rat received a load of tap water by gavage (5% of the body weight), followed by a second load of the same volume with PGZ (n = 12) or vehicle (citric acid, n = 12) 4 hr later. Thirty minutes after the second load, spontaneously voided urine was collected over 90 min. In the ACZ group, ACZ (100 mg/kg BW) was given orally with PGZ (n = 11) or the vehicle (n = 12). At the end of the experiment, blood samples were drawn through cardiac puncture in anesthetized rats. Serum and urine data were measured by the SRL clinical service. Renal clearance (C) was calculated by a standard formula (C = UV/P) and CH_2O was calculated by the following formula: CH_2O = (1 − Uosm/Posm) × UV, where Uosm and Posm denote osmolality of urine and plasma, respectively. $FELi^+$ was calculated as CLi^+/CCr. The blood pressure of restrained conscious rats was measured by a programmed tail-cuff sphygmomanometer (BP-98A; Softron).

Measurement of NHE1 Activity

EF cells from wild-type and $PPAR\gamma^{-/-}$ mice were harvested from 13.5 dpc embryos and were maintained in DMEM supplemented with 10% fetal bovine serum (FBS) as described (Klinghoffer et al., 1999). EF cells derived from mouse embryos deficient in c-Src, Yes, and Fyn ($Src^{-/-}$) or from embryos lacking both Yes and Fyn, but maintaining normal levels of c-Src ($Src^{+/+}$), were obtained from American Type Culture Collection. When cells reached confluency, they were trypsinized and seeded onto 6 mm round coverslips. Cell-coated coverslips were incubated with HEPES-buffered Ringer solution containing BCECF/AM for 30–60 min at room temperature. The coverslip was then superfused with prewarmed (38°C) experimental solutions at ~5 ml/min. The NHE1 activity was determined as described (Haworth et al., 2003). Briefly, the HEPES solution was changed to another solution containing 20 mM NH_4Cl (instead of the equimolar NaCl) for several minutes. The reintroduction of the HEPES solution typically induced pH_i to decrease to a level around pH 6.7 and thereafter, pH_i started to recover from intracellular acidosis. This pH_i recovery reflects the NHE1 activity, because it was almost completely inhibited by 3 μM HOE642 (Sanofi Aventis), a specific inhibitor of NHE1. The NHE1 activity was estimated by calculating the rate of pH_i recovery at fixed pH_i of 6.9 during the recovery from intracellular acidosis.

Adenovirus-Mediated Gene Transfer

The full-length mouse PPARγ1 expression vector for adenovirus-mediated gene transfer was constructed by using AdEasy Vector system (Promega) and pCMX-PPARγ1 (kindly provided by Dr. B. M. Spiegelman) according to the manufacturer's instructions. In addition, the hemagglutinin (HA)-tagged LBD of PPARγ, corresponding to amino acids 184–475, and the LBD containing Q284P mutation, which is devoid of the binding affinity for TZDs (Sarraf et al., 1999), were constructed by PCR-based site-directed mutagenesis (Stratagene) and confirmed by DNA sequencing. These constructs were also subcloned into the adenovirus vector. The EF cells were infected with each recombinant virus at a multiplicity of infection of 220 plaque-forming units/cell, and 48 hr later pH_i measurement was performed.

Antibodies

The anti-PPARγ antibodies were from Santa Cruz Biotechnology, the rabbit anti-HA was from Bethyl Laboratories, and the rabbit and mouse anti-Src were from Cell Signaling Technology. Antibodies against total ERK, phospho-ERK (P-ERK), nonphospho-Src (NP-Src), and phospho-Src (P-Src, tyrosine-416) were from Cell Signaling Technology. The horseradish peroxidase (HRP)-conjugated anti-rabbit or anti-mouse IgG were from Jackson ImmunoResearch Laboratories. Alexa Fluor 488 anti-rabbit IgG and Alexa Fluor 568 phalloidin were from Molecular Probes and 4′,6-diamidino-2-phenylindole dihydrochloride (DAPI) was from Boehringer Mannheim.

Immunoblotting and Immunoprecipitation

For detection of PPARγ, kidney tissues or cell samples were homogenized in ice-cold buffer containing 280 mmol/L sucrose and complete protease inhibitor cocktail (Roche). For detection of PPARγ in PTs, human PTs of ~1 mm length were manually dissected from thin kidney slices and were homogenized in the same buffer. For detection of phosphorylation of ERK or Src, thin slices of kidney cortex were obtained. They were divided into pieces of small bundles consisting mostly of PTs as described (Li et al., 2008). These samples were incubated at 37°C for 40 min in DMEM under 5% CO_2 in the absence or presence of several inhibitors. After TZDs were added for the indicated time, samples were homogenized in ice-cold lysis buffer containing 25 mM Tris-HCl (pH 7.4), 10 mM sodium orthovanadate, 10 mM sodium pyrophosphate, 100 mM sodium fluoride, 10 mM EDTA, 10 mM EGTA, and 1 mM phenylmethylsulfonyl fluoride. For detection of in vivo ERK phosphorylation, rats were sacrificed with excessive amounts of pentobarbital and kidney cortex samples were immediately homogenized in the lysis buffer. Equal amounts of protein samples were obtained from the supernatants, separated by SDS-PAGE on 7% acrylamide minigels, and transferred to a nitrocellulose membrane. After incubation in blocking buffer, the membrane was treated with one of the primary antibodies and then with their respective secondary antibodies. The signal was detected by an ECL Plus system (Amersham).

EF cells were grown on a 10 cm culture dish and FBS was removed overnight. Thereafter, cells were incubated for 40 min in the absence and presence of several inhibitors. After TZDs were added for the indicated time, cells were collected, lysed with the lysis buffer, and subjected to immunoblotting. For immunoprecipitation with PPARγ or Src, the cell lysate was precleaned by incubation with Protein G Sepharose 4 Fast Flow (GE Healthcare Bio-Science) and incubated with the mouse anti-PPARγ or the mouse anti-Src antibodies coupled to Protein G Sepharose 4 Fast Flow. The immunoprecipitates were washed three to five times with the lysis buffer containing 1% Nonidet P-40 and subjected to immunoblotting with the rabbit anti-PPARγ or the rabbit anti-Src antibody. For immunoprecipitation with HA, the rabbit anti-HA antibody was coupled to Protein A Sepharose 4 Fast Flow (GE Healthcare Bio-Science) and immunoblotting was performed with the rabbit anti-HA or the rabbit anti-Src antibody.

Immunohistochemical Analysis

To examine the intrarenal expression of PPARγ, we fixed the kidney samples from humans and rabbits with buffered 4% paraformaldehyde (PFA), sectioned them 5 μm thick in the cryostat at −25°C, air-dried them, and immersed them in PBS, which was followed by incubation with anti-PPARγ (1:100 dilution) overnight at 4°C. The specimens were subsequently incubated with the mixtures of Alexa Fluor 488 anti-rabbit or anti-goat IgG, Alexa Fluor 568 phalloidin for labeling of F-actin, and DAPI for labeling of nuclei for 60 min at room temperature. The kidneys from rats and mice were frozen without fixation and cryosectioned at 10 μm thick and then fixed with buffered 4% PFA for 10 min. After being washed with PBS, sections were serially incubated with anti-PPARγ (1:50) for 1 hr and the mixtures of Cy5-conjugated anti-rabbit IgG, Alexa Fluor 568 phalloidin, and SYBR Green I for nuclei for 30 min at room temperature. An absorption test was performed in the presence of antigen peptide (10 mg/L). The specimens were observed with a confocal laser scanning microscope (MRC-1024K; Japan Bio-Rad Laboratories or LSM510META, Carl Zeiss). For the determination of intrarenal ERK phosphorylation, the antiphospho-ERK and Alexa Fluor 488 anti-rabbit IgG were used. To examine the expression of endogenous PPARγ or exogenous PPARγ constructs in EF cells, we fixed the cells with buffered 4% PFA and processed them for immunostaining as described above by using the anti-PPARγ antibody or the anti-HA antibody as the primary antibody.

Adipocyte Differentiation

EF cells were plated on six-well plastic dishes and propagated to confluence. Two days later, medium was replaced with standard differentiation medium containing 0.5 mM 3-isobutyl-1-methylxanthine, 10 μM dexamethasone, 0.86 μM insulin, 0.3 μM PGZ, and 10% FBS. After 8 days, cells were harvested. The TG levels in the cell lysates were quantified by using the Triglyceride E-test Wako kit (Wako Pure Chemical) according to the manufacturer's protocol.

Statistical Analysis

Data are means ± SEM. Significant differences were determined by applying Student's t test or ANOVA with Bonferroni's adjustment as appropriate. Statistical significance was set at $p < 0.05$.

SUPPLEMENTAL INFORMATION

Supplemental Information includes five figures and can be found with this article online at doi:10.1016/j.cmet.2011.02.015.

ACKNOWLEDGMENTS

This study was supported in part by grants from the Ministry of Education, Culture, Sports, Science and Technology of Japan and in part by a grant from Takeda Pharmaceutical Co., Ltd. The authors thank Ms. Tomoko Miura (Department of Anatomy, Kyorin University School of Medicine) for technical assistance.

Received: September 14, 2010
Revised: January 10, 2011
Accepted: February 17, 2011
Published: May 3, 2011

REFERENCES

Burgermeister, E., and Seger, R. (2008). PPARgamma and MEK interactions in cancer. PPAR Res. *2008*, 309469.

Burgermeister, E., Tencer, L., and Liscovitch, M. (2003). Peroxisome proliferator-activated receptor-γ upregulates caveolin-1 and caveolin-2 expression in human carcinoma cells. Oncogene *22*, 3888–3900.

Chen, L., Yang, B., McNulty, J.A., Clifton, L.G., Binz, J.G., Grimes, A.M., Strum, J.C., Harrington, W.W., Chen, Z., Balon, T.W., et al. (2005). GI262570, a peroxisome proliferator-activated receptor γ agonist, changes electrolytes and water reabsorption from the distal nephron in rats. J. Pharmacol. Exp. Ther. *312*, 718–725.

de Rouffignac, C., Elalouf, J.M., and Roinel, N. (1991). Glucagon inhibits water and NaCl transports in the proximal convoluted tubule of the rat kidney. Pflugers Arch. *419*, 472–477.

Deng, L.J., Wang, F., and Li, H.D. (2005). Effect of gemfibrozil on the pharmacokinetics of pioglitazone. Eur. J. Clin. Pharmacol. *61*, 831–836.

Dewar, B.J., Gardner, O.S., Chen, C.S., Earp, H.S., Samet, J.M., and Graves, L.M. (2007). Capacitative calcium entry contributes to the differential transactivation of the epidermal growth factor receptor in response to thiazolidinediones. Mol. Pharmacol. *72*, 1146–1156.

Friday, E., Oliver, R., 3rd, Welbourne, T., and Turturro, F. (2007). Role of epidermal growth factor receptor (EGFR)-signaling versus cellular acidosis via Na^+/H^+ exchanger1(NHE1)-inhibition in troglitazone-induced growth arrest of breast cancer-derived cells MCF-7. Cell. Physiol. Biochem. *20*, 751–762.

Gonzalez-Campoy, J.M., Romero, J.C., and Knox, F.G. (1989). Escape from the sodium-retaining effects of mineralocorticoids: role of ANF and intrarenal hormone systems. Kidney Int. *35*, 767–777.

Guan, Y., Zhang, Y., Davis, L., and Breyer, M.D. (1997). Expression of peroxisome proliferator-activated receptors in urinary tract of rabbits and humans. Am. J. Physiol. *273*, F1013–F1022.

Guan, Y., Hao, C., Cha, D.R., Rao, R., Lu, W., Kohan, D.E., Magnuson, M.A., Redha, R., Zhang, Y., and Breyer, M.D. (2005). Thiazolidinediones expand body fluid volume through PPARgamma stimulation of ENaC-mediated renal salt absorption. Nat. Med. *11*, 861–866.

Haworth, R.S., McCann, C., Snabaitis, A.K., Roberts, N.A., and Avkiran, M. (2003). Stimulation of the plasma membrane Na^+/H^+ exchanger NHE1 by sustained intracellular acidosis. Evidence for a novel mechanism mediated by the ERK pathway. J. Biol. Chem. *278*, 31676–31684.

Higgins, L.S., and Depaoli, A.M. (2010). Selective peroxisome proliferator-activated receptor γ (PPARgamma) modulation as a strategy for safer therapeutic PPARgamma activation. Am. J. Clin. Nutr. *91*, 267S–272S.

Hirsch, I.B., Kelly, J., and Cooper, S. (1999). Pulmonary edema associated with troglitazone therapy. Arch. Intern. Med. *159*, 1811.

Holthouser, K.A., Mandal, A., Merchant, M.L., Schelling, J.R., Delamere, N.A., Valdes, R.R., Jr., Tyagi, S.C., Lederer, E.D., and Khundmiri, S.J. (2010). Ouabain stimulates Na-K-ATPase through a sodium/hydrogen exchanger-1 (NHE-1)-dependent mechanism in human kidney proximal tubule cells. Am. J. Physiol. Renal Physiol. *299*, F77–F90.

Hong, G., Lockhart, A., Davis, B., Rahmoune, H., Baker, S., Ye, L., Thompson, P., Shou, Y., O'Shaughnessy, K., Ronco, P., and Brown, J. (2003). PPARgamma activation enhances cell surface ENaCalpha via up-regulation of SGK1 in human collecting duct cells. FASEB J. *17*, 1966–1968.

Karalliedde, J., Buckingham, R., Starkie, M., Lorand, D., Stewart, M., and Viberti, G.; Rosiglitazone Fluid Retention Study Group. (2006). Effect of various diuretic treatments on rosiglitazone-induced fluid retention. J. Am. Soc. Nephrol. *17*, 3482–3490.

Kiley, S.C., and Chevalier, R.L. (2007). Species differences in renal Src activity direct EGF receptor regulation in life or death response to EGF. Am. J. Physiol. Renal Physiol. *293*, F895–F903.

Klinghoffer, R.A., Sachsenmaier, C., Cooper, J.A., and Soriano, P. (1999). Src family kinases are required for integrin but not PDGFR signal transduction. EMBO J. *18*, 2459–2471.

Kousteni, S., Bellido, T., Plotkin, L.I., O'Brien, C.A., Bodenner, D.L., Han, L., Han, K., DiGregorio, G.B., Katzenellenbogen, J.A., Katzenellenbogen, B.S., et al. (2001). Nongenotropic, sex-nonspecific signaling through the estrogen or androgen receptors: dissociation from transcriptional activity. Cell *104*, 719–730.

Krieter, P.A., Colletti, A.E., Doss, G.A., and Miller, R.R. (1994). Disposition and metabolism of the hypoglycemic agent pioglitazone in rats. Drug Metab. Dispos. *22*, 625–630.

Kubota, N., Terauchi, Y., Miki, H., Tamemoto, H., Yamauchi, T., Komeda, K., Satoh, S., Nakano, R., Ishii, C., Sugiyama, T., et al. (1999). PPAR γ mediates high-fat diet-induced adipocyte hypertrophy and insulin resistance. Mol. Cell *4*, 597–609.

Li, L., Haynes, M.P., and Bender, J.R. (2003). Plasma membrane localization and function of the estrogen receptor alpha variant (ER46) in human endothelial cells. Proc. Natl. Acad. Sci. USA *100*, 4807–4812.

Li, L., Hisamoto, K., Kim, K.H., Haynes, M.P., Bauer, P.M., Sanjay, A., Collinge, M., Baron, R., Sessa, W.C., and Bender, J.R. (2007). Variant estrogen receptor-c-Src molecular interdependence and c-Src structural requirements for endothelial NO synthase activation. Proc. Natl. Acad. Sci. USA *104*, 16468–16473.

Li, Y., Yamada, H., Kita, Y., Kunimi, M., Horita, S., Suzuki, M., Endo, Y., Shimizu, T., Seki, G., and Fujita, T. (2008). Roles of ERK and cPLA2 in the angiotensin II-mediated biphasic regulation of Na^+-HCO_3^- transport. J. Am. Soc. Nephrol. *19*, 252–259.

Lösel, R., and Wehling, M. (2003). Nongenomic actions of steroid hormones. Nat. Rev. Mol. Cell Biol. *4*, 46–56.

Mudaliar, S., Chang, A.R., and Henry, R.R. (2003). Thiazolidinediones, peripheral edema, and type 2 diabetes: incidence, pathophysiology, and clinical implications. Endocr. Pract. *9*, 406–416.

Müller-Berger, S., Coppola, S., Samarzija, I., Seki, G., and Frömter, E. (1997). Partial recovery of in vivo function by improved incubation conditions of isolated renal proximal tubule. I. Change of amiloride-inhibitable K^+ conductance. Pflugers Arch. *434*, 373–382.

Müller-Berger, S., Samarzija, I., Kunimi, M., Yamada, H., Frömter, E., and Seki, G. (1999). A stop-flow microperfusion technique for rapid determination of HCO_3^- absorption/H^+ secretion by isolated renal tubules. Pflugers Arch. *439*, 208–215.

Muto, S., Miyata, Y., Imai, M., and Asano, Y. (2001). Troglitazone stimulates basolateral rheogenic Na^+/HCO_3^- cotransport activity in rabbit proximal straight tubules. Exp. Nephrol. *9*, 191–197.

Nofziger, C., Chen, L., Shane, M.A., Smith, C.D., Brown, K.K., and Blazer-Yost, B.L. (2005). PPARgamma agonists do not directly enhance basal or insulin-stimulated Na+ transport via the epithelial Na+ channel. Pflugers Arch. *451*, 445–453.

Oliver, R., 3rd, Friday, E., Turturro, F., Lacy, A., and Welbourne, T. (2005). Troglitazone's rapid and sustained activation of ERK1/2 induces cellular acidosis in LLC-PK1-F^+ cells: physiological responses. Am. J. Physiol. Renal Physiol. *288*, F1257–F1266.

Ryan, M.J., Didion, S.P., Mathur, S., Faraci, F.M., and Sigmund, C.D. (2004). PPARγ agonist rosiglitazone improves vascular function and lowers blood pressure in hypertensive transgenic mice. Hypertension *43*, 661–666.

Saad, S., Agapiou, D.J., Chen, X.M., Stevens, V., and Pollock, C.A. (2009). The role of Sgk-1 in the upregulation of transport proteins by PPAR-γ agonists in human proximal tubule cells. Nephrol. Dial. Transplant. *24*, 1130–1141.

Sarraf, P., Mueller, E., Smith, W.M., Wright, H.M., Kum, J.B., Aaltonen, L.A., de la Chapelle, A., Spiegelman, B.M., and Eng, C. (1999). Loss-of-function mutations in PPAR γ associated with human colon cancer. Mol. Cell *3*, 799–804.

Shalmi, M., and Thomsen, K. (1989). Alterations of lithium clearance in rats by different modes of lithium administration. Ren. Physiol. Biochem. *12*, 273–280.

Song, J., Knepper, M.A., Hu, X., Verbalis, J.G., and Ecelbarger, C.A. (2004). Rosiglitazone activates renal sodium- and water-reabsorptive pathways and lowers blood pressure in normal rats. J. Pharmacol. Exp. Ther. *308*, 426–433.

Thomas, J.A., Buchsbaum, R.N., Zimniak, A., and Racker, E. (1979). Intracellular pH measurements in Ehrlich ascites tumor cells utilizing spectroscopic probes generated in situ. Biochemistry *18*, 2210–2218.

Tontonoz, P., Hu, E., and Spiegelman, B.M. (1994). Stimulation of adipogenesis in fibroblasts by PPARγ2, a lipid-activated transcription factor. Cell *79*, 1147–1156.

Vallon, V., Hummler, E., Rieg, T., Pochynyuk, O., Bugaj, V., Schroth, J., Dechenes, G., Rossier, B., Cunard, R., and Stockand, J. (2009). Thiazolidinedione-induced fluid retention is independent of collecting duct alphaENaC activity. J. Am. Soc. Nephrol. *20*, 721–729.

Yamada, H., Seki, G., Taniguchi, S., Uwatoko, S., Nosaka, K., Suzuki, K., and Kurokawa, K. (1996). Roles of Ca^{2+} and PKC in regulation of acid/base transport in isolated proximal tubules. Am. J. Physiol. *271*, F1068–F1076.

Yki-Järvinen, H. (2004). Thiazolidinediones. N. Engl. J. Med. *351*, 1106–1118.

Zanchi, A., Chiolero, A., Maillard, M., Nussberger, J., Brunner, H.R., and Burnier, M. (2004). Effects of the peroxisomal proliferator-activated receptor-γ agonist pioglitazone on renal and hormonal responses to salt in healthy men. J. Clin. Endocrinol. Metab. *89*, 1140–1145.

Zhang, H., Zhang, A., Kohan, D.E., Nelson, R.D., Gonzalez, F.J., and Yang, T. (2005). Collecting duct-specific deletion of peroxisome proliferator-activated receptor γ blocks thiazolidinedione-induced fluid retention. Proc. Natl. Acad. Sci. USA *102*, 9406–9411.

Zhang, F., Lavan, B.E., and Gregoire, F.M. (2007). Selective modulators of PPAR-gamma activity: molecular aspects related to obesity and side-effects. PPAR Res. *2007*, 32696.

Zheng, Y., Horita, S., Hara, C., Kunimi, M., Yamada, H., Sugaya, T., Goto, A., Fujita, T., and Seki, G. (2003). Biphasic regulation of renal proximal bicarbonate absorption by luminal AT1A receptor. J. Am. Soc. Nephrol. *14*, 1116–1122.

Apoptosis inhibitor of macrophage (AIM) is required for obesity-associated recruitment of inflammatory macrophages into adipose tissue

Jun Kurokawa[a], Hiromichi Nagano[a], Osamu Ohara[b], Naoto Kubota[c], Takashi Kadowaki[c], Satoko Arai[a], and Toru Miyazaki[a,1]

[a]Laboratory of Molecular Biomedicine for Pathogenesis, Center for Disease Biology and Integrative Medicine, Faculty of Medicine, University of Tokyo, Tokyo 113-0033, Japan; [b]Department of Human Genome Research, Kazusa DNA Research Institute, Kisarazu, Chiba 292-0818, Japan; and [c]Department of Internal Medicine, Graduate School of Medicine, University of Tokyo, Tokyo 113-0033, Japan

Edited* by Tadatsugu Taniguchi, University of Tokyo, Tokyo, Japan, and approved June 14, 2011 (received for review February 3, 2011)

Infiltration of inflammatory macrophages into adipose tissues with the progression of obesity triggers insulin resistance and obesity-related metabolic diseases. We recently reported that macrophage-derived apoptosis inhibitor of macrophage (AIM) protein is increased in blood in line with obesity progression and is incorporated into adipocytes, thereby inducing lipolysis in adipose tissue. Here we show that such a response is required for the recruitment of adipose tissue macrophages. In vitro, AIM-dependent lipolysis induced an efflux of palmitic and stearic acids from 3T3-L1 adipocytes, thereby stimulating chemokine production in adipocytes via activation of toll-like receptor 4 (TLR4). In vivo administration of recombinant AIM to *TLR4*-deficient ($TLR4^{-/-}$) mice resulted in induction of lipolysis without chemokine production in adipose tissues. Consistently, mRNA levels for the chemokines that affect macrophages were far lower in *AIM*-deficient ($AIM^{-/-}$) than in wild-type ($AIM^{+/+}$) obese adipose tissue. This reduction in chemokine production resulted in a marked prevention of inflammatory macrophage infiltration into adipose tissue in obese $AIM^{-/-}$ mice, although these mice showed more advanced obesity than $AIM^{+/+}$ mice on a high-fat diet. Diminished macrophage infiltration resulted in decreased inflammation locally and systemically in obese $AIM^{-/-}$ mice, thereby protecting them from insulin resistance and glucose intolerance. These results indicate that the increase in blood AIM is a critical event for the initiation of macrophage recruitment into adipose tissue, which is followed by insulin resistance. Thus, AIM suppression might be therapeutically applicable for the prevention of obesity-related metabolic disorders.

diabetes | fatty acid synthase | CD36 | knockout mouse

Chronic, low-grade inflammation observed in adipose tissues is characteristic of obesity. Such a subclinical inflammatory state of adipose tissues is highly associated with insulin resistance both in adipose tissue and systemically and thus contributes to the development of multiple obesity-induced metabolic and cardiovascular diseases (1–4). Evidence has shown that infiltration of a large number of classically activated inflammatory macrophages (M1 macrophages) into adipose tissue is responsible for obesity-associated inflammation (5–7). Lean adipose tissue contains a resident population of alternatively activated macrophages (M2 macrophages), which can suppress the inflammation of both adipocytes and macrophages partly via the secretion of interleukin (IL)-10. Hence, obesity induces a switch in macrophage activation state in adipose tissue toward M1 polarization, which leads to inflammation (8–12). However, the mechanism that promotes infiltration of inflammatory macrophages into obese adipose tissue is as yet unknown.

We recently reported that the apoptosis inhibitor of macrophage (AIM) protein (13) is incorporated into adipocytes via CD36-mediated endocytosis, and induces lipolysis by suppressing the activity of fatty acid synthase (FAS) (14). AIM is a member of the scavenger receptor cysteine-rich superfamily and was initially identified as an apoptosis inhibitor that supports the survival of macrophages against different types of apoptosis-inducing stimuli (13). AIM is a direct target for regulation by nuclear receptor liver X receptor/retinoid X receptor (LXR/RXR) heterodimers (15, 16) and is solely produced by tissue macrophages. As a secreted molecule, AIM is detected in both human and mouse blood at various levels (13, 16–19) and increases in blood with the progression of obesity in mice fed a high-fat diet (HFD) (14). The augmented blood AIM induced lipolysis, as evident by the fact that the increase of free fatty acids (FFAs) and glycerol in blood was suppressed in $AIM^{-/-}$ mice (14). Owing to less lipolysis, adipocyte hypertrophy was more advanced and the overall mass of visceral adipose tissues was greater in $AIM^{-/-}$ than in $AIM^{+/+}$ mice fed a HFD (14). All these observations imply that AIM-induced lipolysis might be responsible for the obesity-associated recruitment of adipose tissue macrophages.

In the present study, we assessed whether AIM affects macrophage accumulation in adipose tissues in obese mice. In addition, we determined the molecular mechanism of how AIM-dependent lipolysis results in the production of chemokines by adipocytes for the effective recruitment of adipose tissue macrophages. Finally, we investigated how the absence of AIM influences the local and systemic inflammatory state and insulin resistance in mice. On the basis of these results, we discuss the putative role of AIM in the initiation of obesity-associated chronic inflammation and subsequent metabolic diseases.

Results and Discussion

Prevention of M1 Macrophage Recruitment into Adipose Tissues in Obese $AIM^{-/-}$ Mice. In $AIM^{-/-}$ mice, adipocyte hypertrophy was more advanced than in $AIM^{+/+}$ mice, and the overall mass of visceral fat as well as body weight was markedly greater compared with that of $AIM^{+/+}$ mice (14). Interestingly, however, far fewer macrophages stained with a pan-macrophage antibody F4/80 were observed in epididymal adipose tissue in $AIM^{-/-}$ mice than in $AIM^{+/+}$ mice fed a HFD for 12 wk (Fig. 1*A*). The number of IL-6 stained inflammatory type (M1) macrophages in obese $AIM^{-/-}$ mice was markedly lower than in obese $AIM^{+/+}$ mice (Fig. 1*A*). In addition, almost no M1 macrophage clusters forming crown-like structures (CLS) were observed in obese $AIM^{-/-}$ mice (Fig. 1*A*). In contrast, the number of M2 adipose tissue macrophages stained for mannose receptor (MR) was not increased in $AIM^{+/+}$ or $AIM^{-/-}$ mice after a 12-wk HFD (Fig. 1*B*). Furthermore, the stromal-vascular cell fraction (SVF) containing macrophages was isolated from the epididymal fat tissue of lean and obese mice by collagenase treatment and

Author contributions: T.M. designed research; J.K., O.O., N.K., and S.A. performed research; H.N. contributed new reagents/analytic tools; J.K., O.O., T.K., and T.M. analyzed data; and S.A. and T.M. wrote the paper.

The authors declare no conflict of interest.

*This Direct Submission article had a prearranged editor.

[1]To whom correspondence should be addressed. E-mail: tm@m.u-tokyo.ac.jp.

This article contains supporting information online at www.pnas.org/lookup/suppl/doi:10.1073/pnas.1101841108/-/DCSupplemental.

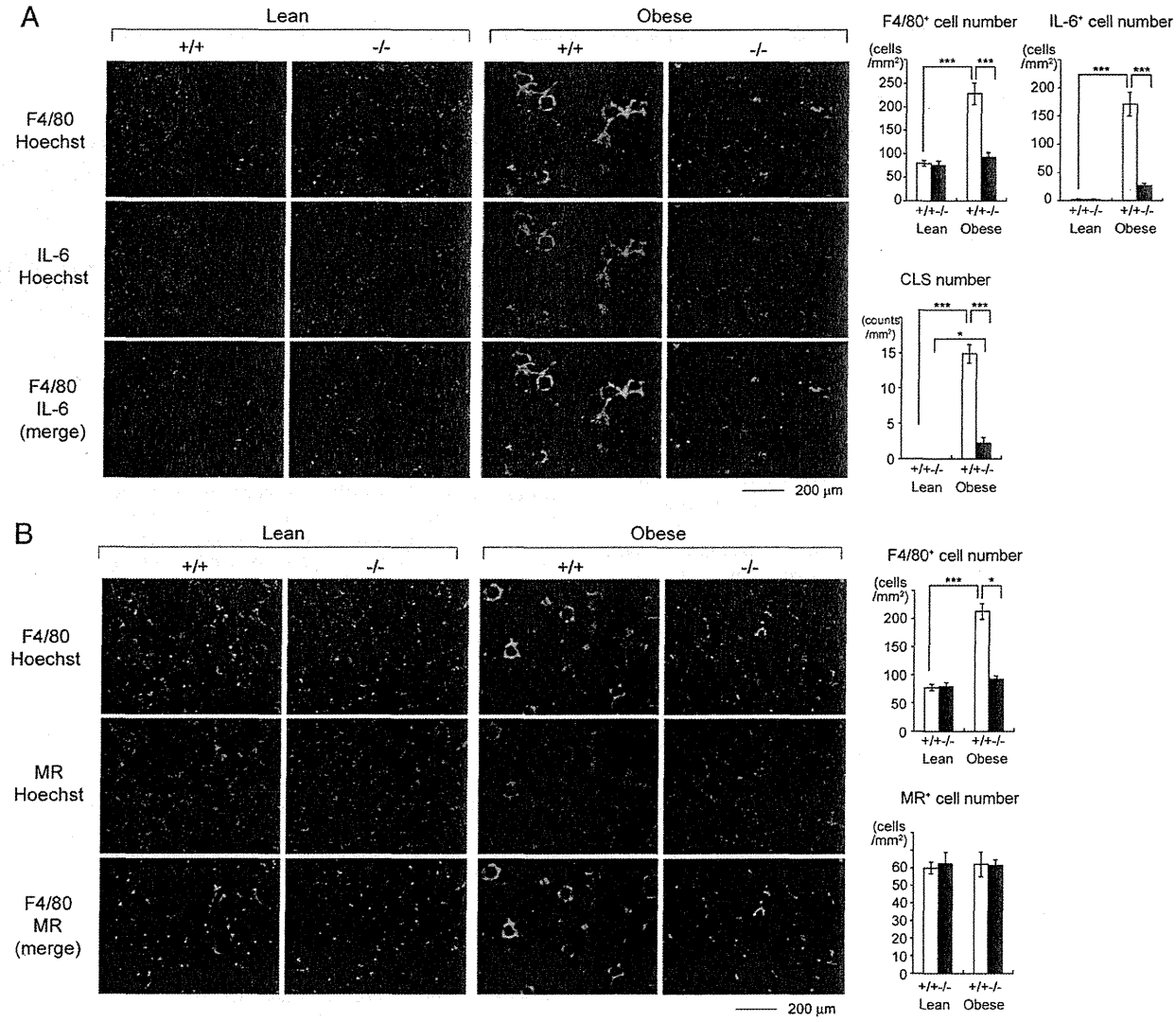

Fig. 1. Requirement of AIM for macrophage recruitment into obese adipose tissue. (*A* and *B*) Specimens of epididymal fat tissue from lean (0 wk) or obese (fed a HFD for 12 wk) $AIM^{+/+}$ and $AIM^{-/-}$ mice were costained for F4/80 (pan-macrophage marker; green), IL-6 (red), and Hoechst (blue) for *A*, and F4/80 (pan-macrophage marker; green), mannose receptor (MR) (red), and Hoechst (blue) for *B*. (Scale bar, 200 μm.) Quantification of $F4/80^+$ cell number, $IL\text{-}6^+$ macrophages, and the number of crown-like structures (CLS) are presented for *A*, or $F4/80^+$ cell number and MR^+ macrophages for *B* are presented. At least three different areas in three different sections per mouse were analyzed in six to eight mice of each genotype. Results are presented as averages ± SEM.

assessed to determine the number of both types of macrophage by flow cytometry after staining for F4/80 and CD11b (macrophage), CD11c (M1 marker), and MR. Consistent with the histological data, the increase in M1 macrophage number was apparent in obese $AIM^{+/+}$ but not in obese $AIM^{-/-}$ mice (Fig. S1*A*). The M1/M2 ratio of macrophage number was significantly increased in obese $AIM^{+/+}$ than in lean $AIM^{+/+}$ mice, indicating M1 polarization of adipose tissue macrophage (9), whereas this was comparable in lean and obese $AIM^{-/-}$ mice (Fig. S1*B*). Similarly, quantitative RT-PCR (QPCR) analysis with RNA isolated from epididymal fat showed a remarkable increase in mRNA levels for M1 macrophage marker genes, such as *CD11c* and *iNOS*, after a 12-wk HFD in $AIM^{+/+}$ mice, whereas this was not apparent in $AIM^{-/-}$ mice (Fig. S1*C*). In addition, expression levels of antiinflammatory (M2) macrophage marker genes, such as *CD163*, *MR*, and *arginase*, were decreased in epididymal fat of $AIM^{+/+}$ mice fed a HFD, whereas this was not observed in $AIM^{-/-}$ mice (Fig. S1*C*). The reduction in mRNA levels of M2 markers in obese $AIM^{+/+}$ mice is consistent with the increase in the M1/M2 ratio of macrophage number in obese $AIM^{+/+}$ mice (Fig. 1*D*). The difference in macrophage accumulation in fat in the presence or absence of AIM was not predominantly brought about by the antiapoptotic effect of AIM (13, 20) because the apoptotic state of macrophages (and also of adipocytes) was comparable between obese $AIM^{+/+}$ and $AIM^{-/-}$ epididymal adipose tissues, as assessed by TUNEL staining (Fig. S2). These results implicate an indispensable role of AIM in the obesity-associated recruitment of adipose tissue macrophages.

AIM-Dependent Lipolysis Induces Macrophage Migration. We then tested whether AIM itself attracts macrophages. However, AIM showed no chemoattractive activity in a macrophage migration assay using RAW264.1 mouse macrophage cells (Fig. 2*A*, *Left*). In contrast, conditioned medium from 3T3-L1 adipocytes that had been challenged with rAIM for 72 h (AIM CM) efficiently attracted macrophage cells (Fig. 2*A*, *Left*). A comparable effect was observed with conditioned medium from cells treated with C75, a specific FAS inhibitor that also induces lipolysis (14). AIM CM also attracted

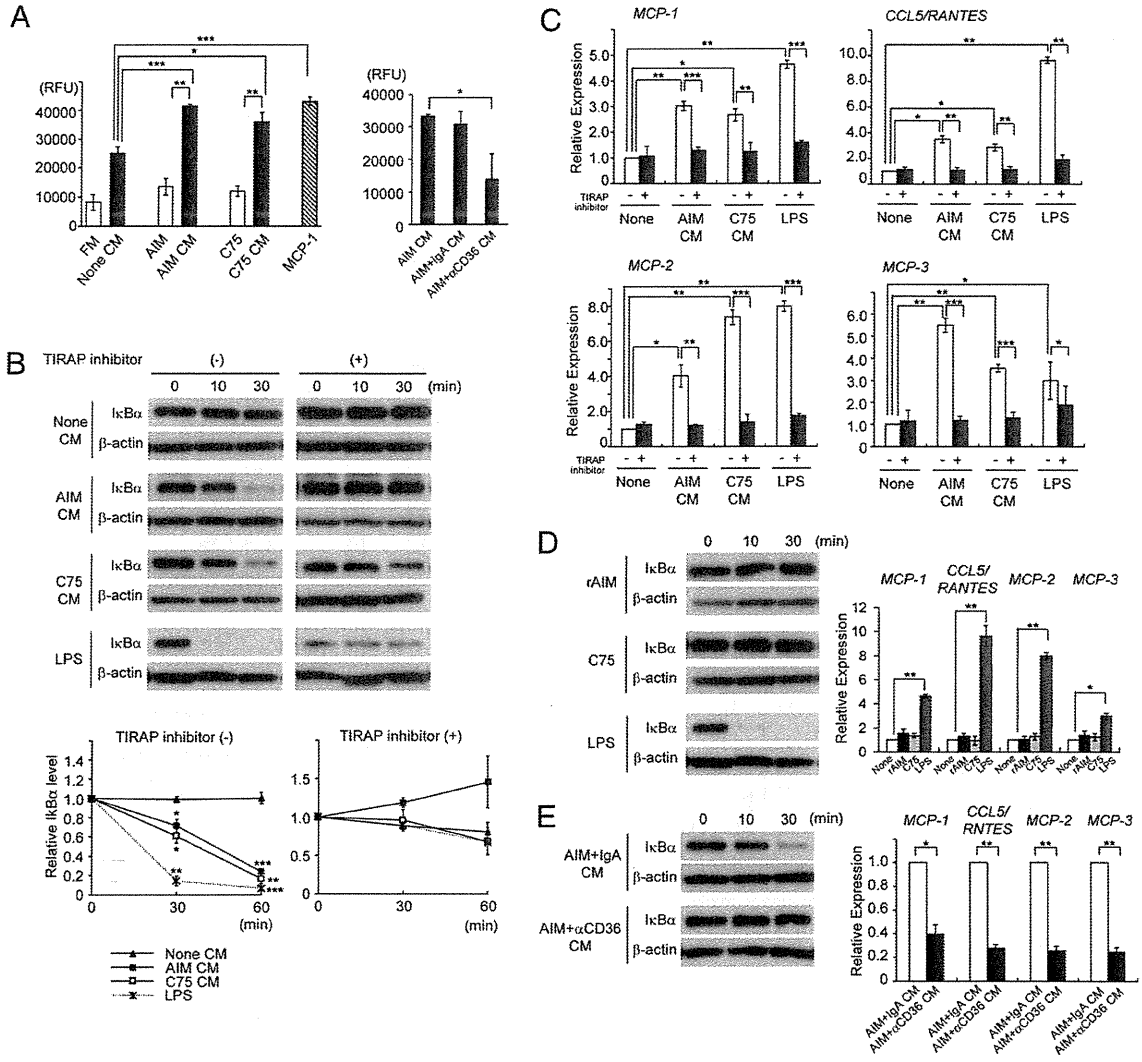

Fig. 2. AIM-dependent lipolysis induces chemokine production in adipocytes via TLR4 stimulation. (*A*) Chemotaxis of RAW 264.1 cells in response to specified stimulant. Attractants: rAIM (25 μg/mL), C75 (25 μM), AIM CM/C75 CM: conditioned medium from 3T3-L1 adipocytes treated for 3 d with rAIM (25 μg/mL) or C75 (25 μM), respectively; AIM+αCD36 CM/AIM+IgA CM: conditioned medium from 3T3-L1 adipocytes treated for 3 d with rAIM (25 μg/mL) in the presence of anti-CD36 Ab or mouse IgA (10 μg/mL each), respectively; none CM, control CM: treated without rAIM or C75; and FM: fresh DMEM culture medium containing 10% FBS. Averages from $n = 3 \pm$ SEM. MCP-1 (100 ng/mL) was used as a positive control. (*B*) Degradation of IkBα in 3T3-L1 adipoctytes in response to specified stimulant in the absence (−) or presence (+) of a TIRAP inhibitor (100 μM). LPS (100 ng/mL) was used as a positive control. Representative immunoblotting results are presented. The density of the signal was quantified using National Institutes of Health Image J image analysis software and presented as values relative to those of prestimulation (*Lower* two panels). $n = 3$. Error bar: SEM. *, versus the value at prestimulation (0 min). (*C*) QPCR analysis of mRNA levels for *MCP-1*, *CCL5/RANTES*, *MCP-2*, and *MCP-3* using RNA isolated from 3T3-L1 adipocytes treated with specified stimulant for 24 h in the absence (white bars) or presence (black bars) of a TIRAP inhibitor. Values were presented as relative expression to those without stimulation (none). $n = 3$ for each. Error bar: SEM. (*D* and *E*) No degradation of IkBα or expression induction of mRNA for chemokine genes in 3T3-L1 adipoctytes in response to rAIM alone (25 μg/mL) (*D*) or AIM+αCD36 CM (*E*).

J774.1 mouse monocyte cells (Fig. S3*A*). Furthermore, 3T3-L1 adipocytes were treated with rAIM in the presence of a CD36-neutralizing antibody (mouse IgA), which inhibits AIM-dependent lipolysis by disturbing the endocytosis of AIM into adipocytes (14), and the conditioned medium (AIM+αCD36 CM) was assessed in the macrophage migration assay. The AIM+αCD36 CM did not efficiently attract macrophages (Fig. 2*A*, *Right*), suggesting that AIM-induced lipolysis in adipocytes appears to be responsible for macrophage recruitment. The CD36-neutralizing antibody itself had no direct effect on the macrophage migration (Fig. S3*B*).

Fatty Acids Effluxed from Adipocytes in Response to AIM-Dependent Lipolysis Stimulated TLR Signaling Pathway and Induced Chemokine Production in Adipocytes. Accumulating evidence has demonstrated that saturated fatty acids activate TLR signaling cascade and that this response is tightly associated with obesity-induced inflammation (21–25). Thus, it is plausible that an increase in blood AIM may induce vigorous lipolysis in obese adipose tissues, and saturated fatty acids effluxed from adipocytes as a result of lipolysis might activate chemokine production in adipocytes via the stimulation of TLR(s) in a paracrine/autocrine fashion (26–28). Indeed, palmitic and stearic acids, the major fatty acids comprising triglyceride droplets (29) and well known as stimulators of TLR4 and TLR2 (21, 25, 30, 31), were identified as the components released by adipocytes in response to lipolysis induced by AIM or C75 when the profile of fatty acids in AIM CM and C75 CM was evaluated by gas-chromatography mass-spectrometry analysis.

Consistent with this result, both AIM CM and C75 CM efficiently stimulated the TLR signaling cascade and chemokine production in 3T3-L1 adipocytes, as assessed by degradation of IkBα (Fig. 2*B*) and mRNA expression of chemokines such as *MCP-1*, *CCL5/RANTES*, *MCP-2*, and *MCP-3*, which affects macrophages (Fig. 2*C*). AIM CM induced substantial levels of protein of these chemokines as assessed by ELISA (Fig. S4*A*). These responses diminished when adipocytes were treated with AIM CM or C75 CM in the presence of a toll–interleukin-1 receptor domain containing adapter protein (TIRAP) inhibitor, which specifically interferes with the interaction of TLR4 (as well as TLR2) and the adapter protein TIRAP/Mal, resulting in attenuation of TLR signaling (Fig. 2 *B* and *C*) (32). Furthermore, we confirmed that similar effects of TLR activation and chemokine production were observed when 3T3-L1 adipocytes were treated with palmitic acid (PA) or stearic acid (SA) and that the responses induced by each fatty acid were reduced when subjected to the TIRAP inhibitor (Fig. S5). Consistent with the results from macrophage migration assay presented in Fig. 2*A*, neither rAIM alone (Fig. 2*D* and Fig. S4*B*) nor AIM+αCD36 CM (Fig. 2*E* and Fig. S4*C*) stimulated IkBα degradation or chemokine mRNA and protein expression in adipocytes. These findings clearly indicate the necessity of the lipolytic process in the overall activation of TLR signaling cascade by AIM.

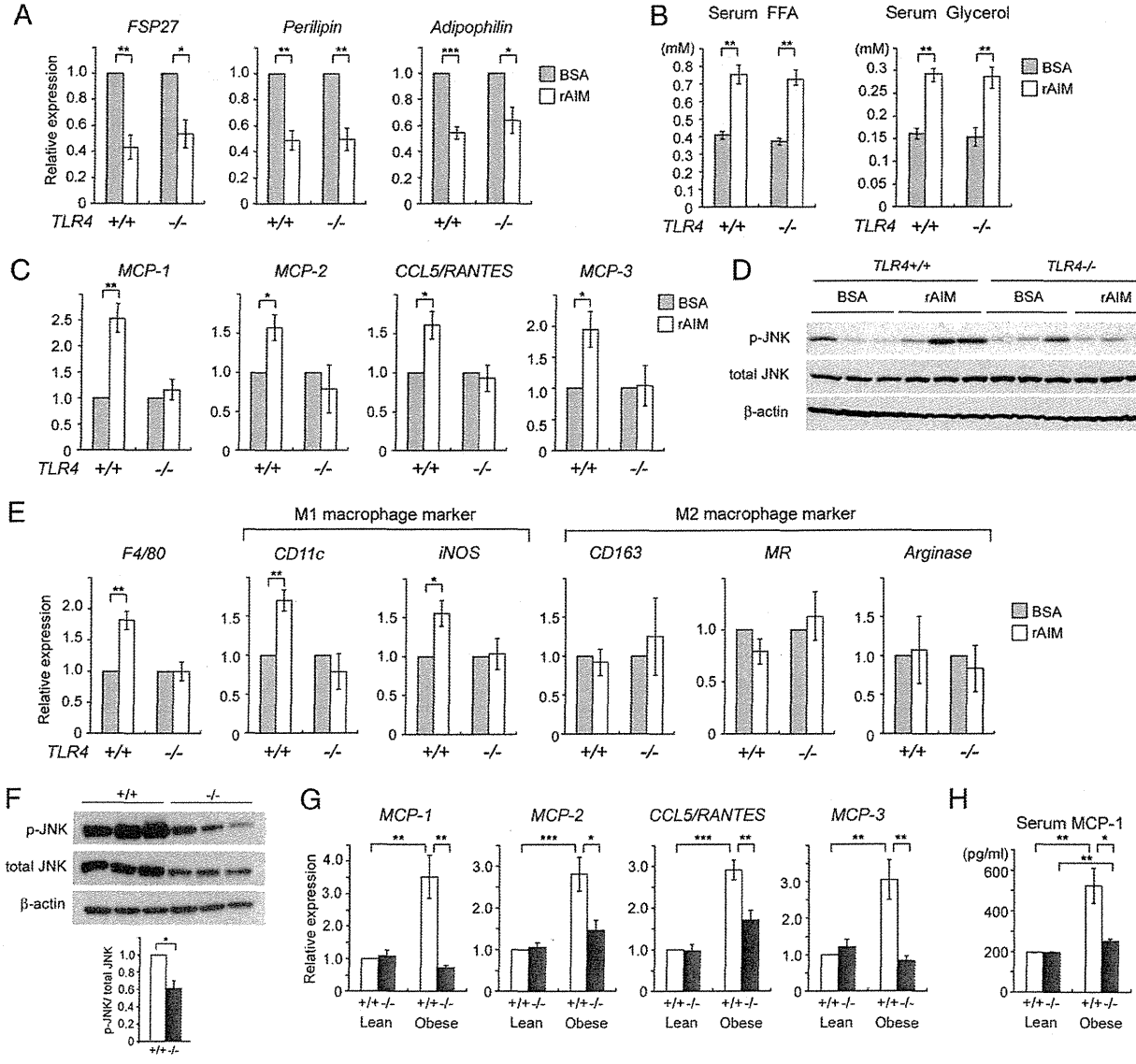

Fig. 3. Involvement of TLR4 in adipose tissue macrophage recruitment by AIM in vivo. (*A–E*) $TLR4^{-/-}$ and wild-type littermate mice (B6 background) were i.v. injected with rAIM or BSA three times every other day (400 μg in 200 μL PBS per injection). The day after the third injection (day 8 from the first injection), mice were killed, and lipolysis, chemokine expression, and adipose tissue macrophage accumulation were analyzed. $n = 5$ for each. (*A*) mRNA levels for *FSP27*, *Perilipin*, and *Adipophilin* were assessed by QPCR using RNA isolated from epididymal fat. Values were presented as relative expression to those of fat tissue injected with BSA. Error bar: SEM. (*B*) Serum levels for FFA and glycerol. (*C*) mRNA levels for chemokines. (*D*) Immunoblotting for total and phosphorylated JNK in epididymal fat. Immunoblot for β-actin is also presented. Results from three mice for each group are presented. Note that comparable results were obtained in five independent mice in each group. (*E*) mRNA levels for F4/80 pan-macrophage marker, M1 and M2 macrophage markers to assess macrophage recruitment. (*F*) Immunoblotting for total and phosphorylated JNK using lysates obtained from epididymal fats of $AIM^{+/+}$ and $AIM^{-/-}$ mice fed a HFD for 12 wk ($n = 4$–6). Relative values of phosphorylated JNK signals to total JNK are also presented (*Lower* graph). (*G*) QPCR analysis of mRNA levels for chemokine genes in epididymal fat tissue and (*H*) serum MCP-1 concentration in $AIM^{+/+}$ and $AIM^{-/-}$ mice fed a HFD for 0 (lean) or 12 wk (obese); $n = 6$–8.

Involvement of TLR4. As TIRAP is downstream of not only TLR4 but also other TLRs, including TLR2 (32), the precise involvement of TLR4 in macrophage recruitment was further verified. We first suppressed *TLR4* expression by siRNA in 3T3-L1 adipocytes and assessed the induction of MCP-1 by AIM CM. As shown in Fig. S6 *A–C*, induction of both mRNA and protein of MCP-1 by AIM CM was significantly reduced in cells transfected with siRNA for *TLR4*. In addition, we injected rAIM i.v. into wild-type and $TLR4^{-/-}$ mice and thereafter assessed the state of lipolysis and chemokine production in epididymal adipose tissue. In both types of mice, the mRNA levels of *FSP27* (also called *Cidec*), *Perilipin*, and *Adipophilin*, coating elements for lipid droplets, were decreased after challenging with rAIM (Fig. 3*A*), a finding consistent with the progression of lipolysis reported previously (17, 33, 34). Similarly, the increase in blood FFA and glycerol levels was equivalent in $TLR4^{-/-}$ and wild-type mice (Fig. 3*B*). In contrast, induction of mRNA for chemokines by rAIM injection was significantly less efficient in $TLR4^{-/-}$ than in wild-type mice (Fig. 3*C*). In line with this, phosphorylation levels of c-Jun N-terminal kinases (JNKs) in epididymal fat, which represent the state of TLR activation, were up-regulated in wild-type mice but not in $TLR4^{-/-}$ mice (Fig. 3*D*). Furthermore, the rAIM injection increased mRNA levels for M1 macrophage markers in epididymal adipose tissue of wild-type but not $TLR4^{-/-}$ mice, demonstrating that AIM-induced lipolysis could not recruit inflammatory macrophages into adipose tissue in the absence of TLR4 (Fig. 3*E*). There was no significant change in mRNA levels for M2 macrophage markers in both $TLR4^{-/-}$ and wild-type mice (Fig. 3*E*). Histological analysis revealed the presence of IL-6 expressing M1 macrophages after the rAIM injection in epididymal adipose tissue of wild-type mice but not of $TLR4^{-/-}$ mice (Fig. S6*D*).

Consistent results were obtained in obese $AIM^{+/+}$ and $AIM^{-/-}$ mice after 12 wk on a HFD. In epididymal fat, phosphorylation levels of JNKs were decreased in $AIM^{-/-}$ mice compared with $AIM^{+/+}$ mice (Fig. 3*F*). In addition, chemokine mRNA levels were also lower in $AIM^{-/-}$ than in $AIM^{+/+}$ adipose tissue (Fig. 3*G*). Moreover, the serum level of MCP-1 was lower in $AIM^{-/-}$ than in $AIM^{+/+}$ mice (Fig. 3*H*).

It is possible that fatty acids effluxed from adipocytes may stimulate TLR4 expressed not only on adipocytes but also on resident M2 macrophages within adipose tissue in a paracrine fashion and may induce chemokine expression in macrophages. To assess this possibility, we stained epididymal fat from wild-type $AIM^{+/+}$ mice fed a HFD for 6 wk for MR, a M2 macrophage marker, and MCP-1. As shown in Fig. S7, both adipocytes and M2 macrophages stained positive for MCP-1. As expected, in $AIM^{-/-}$ mice, neither adipocytes nor resident macrophages showed obvious MCP-1 expression. Thus, in summary, AIM-induced lipolysis provoked the efflux of saturated fatty acids, including palmitic and stearic acids, from adipocytes, and these fatty acids stimulated chemokine production in both adipocytes and resident macrophages via TLR4 activation, resulting in M1 macrophage migration.

Prevention of Obesity-Associated Inflammation and Insulin Resistance in $AIM^{-/-}$ Mice. As a consequence of abolished infiltration of inflammatory macrophages, the progression of obesity-associated inflammation was prevented both locally and systemically in obese $AIM^{-/-}$ mice. In adipose tissue (Fig. 4*A*) and the liver (Fig. S8), mRNA levels for proinflammatory cytokines, such as *TNFα*, *IL-6*, and *IL-1β*, were significantly lower in $AIM^{-/-}$ than in $AIM^{+/+}$ mice after a HFD for 12 wk. Consistent with this finding, serum levels of TNFα and IL-6 were lower in $AIM^{-/-}$ mice compared with $AIM^{+/+}$mice (Fig. 4*B*).

Having observed decreased inflammation in $AIM^{-/-}$ mice, we next assessed insulin sensitivity in $AIM^{-/-}$ and $AIM^{+/+}$ mice fed a HFD for 12 wk. Activation of the insulin signaling pathway after i.v. injection of insulin was studied in adipose tissue, skeletal muscle (gastrocnemius), and liver. As shown in Fig. 4*C*, substantial insulin-stimulated phosphorylation of AKT and GSK3β protein kinases

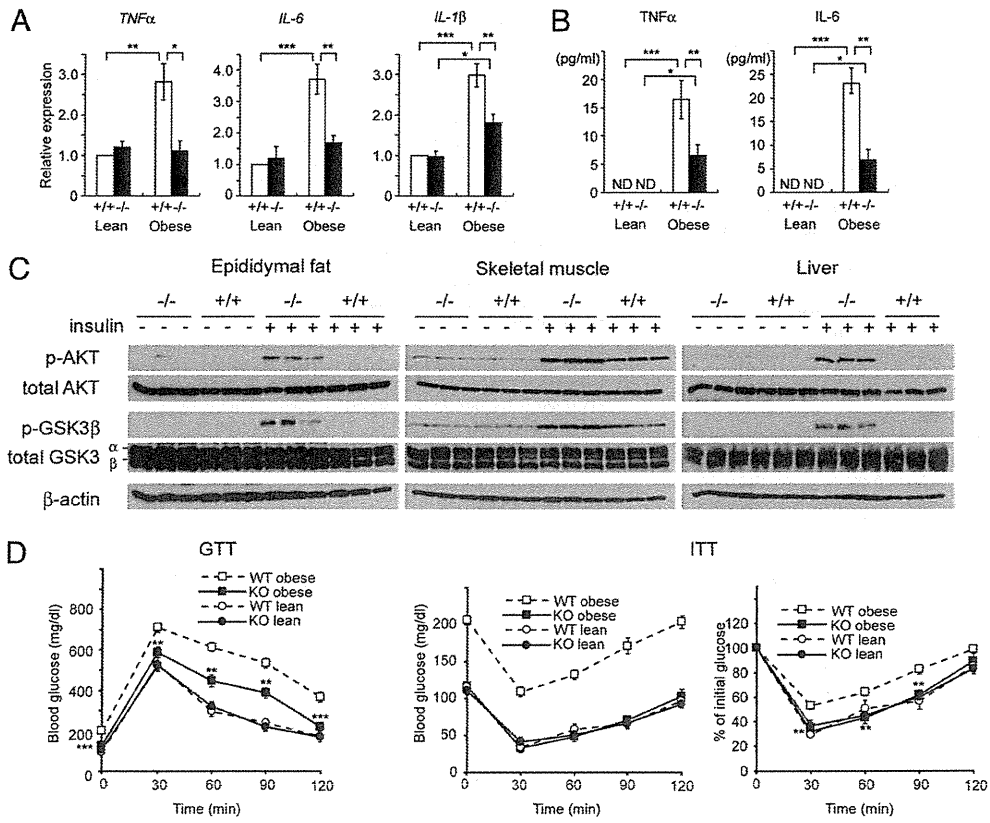

Fig. 4. Prevented inflammation and normal insulin sensitivity in obese $AIM^{-/-}$ mice. (*A*) Local inflammation. QPCR analysis of mRNA levels for inflammatory cytokine genes in epididymal fat tissue from $AIM^{+/+}$ or $AIM^{-/-}$ mice fed a HFD for 0 (lean) or 12 wk (obese). n = 6–8 for each group. Values were presented as relative expression to that in lean $AIM^{+/+}$ mice. Error bar: SEM. (*B*) Systemic inflammation. Serum TNFα and IL-6 levels are the same as in *A*. (*C*) $AIM^{-/-}$ and $AIM^{+/+}$ mice fed a HFD for 12 wk (three mice for each) were fasted for 5 h and treated with insulin (10 U/kg body weight) via i.p. injection. Within 15 min, epididymal fat, skeletal muscle (gastrocnemius), and liver were isolated and examined by immunoblotting for phosphorylated AKT (p-AKT), total AKT, phosphorylated GSK3β (p-GSK3β), total GSK3 (α and β), and β-actin. (*D*) Glucose tolerance test (GTT) and insulin tolerance test (ITT) performed on $AIM^{+/+}$ and $AIM^{-/-}$ mice fed a HFD for 0 (lean) or 12 wk (obese); n = 6–8 for each group. For ITT, two panels including absolute blood glucose levels (*Left*) and % of the initial (time 0) glucose level (*Right*) are presented.

was observed in all three tissues in $AIM^{-/-}$ mice in contrast to the markedly diminished phosphorylation levels in $AIM^{+/+}$ mice. Thus, insulin sensitivity was preserved in obese $AIM^{-/-}$ mice. Consistent with these results, whole-body glucose intolerance and insulin resistance observed in $AIM^{+/+}$ mice were found to be ameliorated in $AIM^{-/-}$ mice by i.p. glucose and insulin tolerance tests (GTT and ITT, respectively; Fig. 4*D*). Insulin production in pancreatic β cells in response to glucose was comparable in $AIM^{-/-}$ and $AIM^{+/+}$ mice, as assessed in vivo (Fig. S8*B*) and in vitro using isolated pancreatic Langerhans islets (Fig. S8*C*).

Conclusion

The present results provide unique and important evidence regarding the role of AIM in the initiation of chronic inflammation that connects obesity and insulin resistance. Firstly, macrophage recruitment into obese adipose tissues requires AIM-induced lipolysis. Augmentation of blood AIM levels may induce vigorous lipolysis in obese adipose tissues, increasing local extracellular fatty acid concentration to a level sufficient for the stimulation of TLR4, which triggers chemokine production by adipocytes and macrophage recruitment (summarized in Fig. S9). Although we and others previously reported some related facts underlying this conclusion, which were observed in a number of different physiological and experimental conditions (12, 14, 21–33), we would like to emphasize that this study, which focused on AIM, has uniquely linked apparently independent elements to a process that occurs during the progression to obesity.

Secondly, adipocyte hypertrophy is not solely sufficient for the initiation of macrophage infiltration; an increase in blood AIM needs to be accompanied. In $AIM^{-/-}$ mice, although the level of AIM-independent lipolysis increases in line with adipocyte hypertrophy (14), it may not reach a level sufficient for macrophage recruitment (Fig. S9). Thirdly, within adipose tissue, crosstalk between macrophages and adipocytes establishes a vicious cycle that accelerates inflammation; saturated fatty acids brought about by lipolysis activate TLR4 to induce TNFα, which in turn activates the TNFα receptor to produce inflammatory cytokines/adipokines and chemokines (35). The end point of this response is further progression of inflammation, lipolysis, and macrophage recruitment. It is likely that via an increase in lipolysis, AIM may strengthen this crosstalk, further contributing to the progression of inflammation (Fig. S9).

Thus, this study might not only advance our knowledge about the events triggering obesity-associated inflammation, but also open a door to the development of next-generation antimetabolic therapies via suppression of AIM.

Materials and Methods

Mice. $AIM^{-/-}$ mice (13) had been backcrossed to C57BL/6 (B6) for 13 generations before used for experiments. HFD (HFD32, fat kcal: 60%) was purchased from CREA. $TLR4^{-/-}$ mice (36) were kindly provided from Drs. S. Akira (Osaka University, Osaka, Japan) and K. Miyake (The Institute of Medical Science, University of Tokyo, Tokyo, Japan). All mice were maintained under a specific pathogen free condition.

Statistical Analysis. A two-tailed Mann-Whitney test was used to calculate *P* values. $***P < 0.001$, $**P < 0.01$, $*P < 0.05$. Error bars: SEM.

Please see *SI Materials and Methods* for further details.

ACKNOWLEDGMENTS. We thank Genostaff Inc. for technical assistance in histology. This work was supported by Grants-in-Aid for Scientific Research (B) (Japan Society for the Promotion of Science), the Global Centers of Excellence (COE) Program (T.M.), Kanae Foundation for the Promotion of Medical Science, the Astellas Foundation for Research on Metabolic Disorders, and the Ono Medical Research Foundation (S.A.).

1. Hotamisligil GS, Shargill N-S, Spiegelman B-M (1993) Adipose expression of tumor necrosis factor-alpha: Direct role in obesity-linked insulin resistance. *Science* 259: 87–91.
2. Wellen KE, Hotamisligil GS (2003) Obesity-induced inflammatory changes in adipose tissue. *J Clin Invest* 112:1785–1788.
3. Arkan MC, et al. (2005) IKK-beta links inflammation to obesity-induced insulin resistance. *Nat Med* 11:191–198.
4. Shoelson SE, Lee J, Goldfine AB (2006) Inflammation and insulin resistance. *J Clin Invest* 116:1793–1801.
5. Weisberg SP, et al. (2003) Obesity is associated with macrophage accumulation in adipose tissue. *J Clin Invest* 112:1796–1808.
6. Xu H, et al. (2003) Chronic inflammation in fat plays a crucial role in the development of obesity-related insulin resistance. *J Clin Invest* 112:1821–1830.
7. Solinas G, et al. (2007) JNK1 in hematopoietically derived cells contributes to diet-induced inflammation and insulin resistance without affecting obesity. *Cell Metab* 6: 386–397.
8. Gordon S, Taylor PR (2005) Monocyte and macrophage heterogeneity. *Nat Rev Immunol* 5:953–964.
9. Lumeng CN, Bodzin JL, Saltiel AR (2007) Obesity induces a phenotypic switch in adipose tissue macrophage polarization. *J Clin Invest* 117:175–184.
10. Ozcan U, et al. (2004) Endoplasmic reticulum stress links obesity, insulin action, and type 2 diabetes. *Science* 306:457–461.
11. Kahn SE, Hull RL, Utzschneider KM (2006) Mechanisms linking obesity to insulin resistance and type 2 diabetes. *Nature* 444:840–846.
12. Kosteli A, et al. (2010) Weight loss and lipolysis promote a dynamic immune response in murine adipose tissue. *J Clin Invest* 120:3466–3479.
13. Miyazaki T, Hirokami Y, Matsuhashi N, Takatsuka H, Naito M (1999) Increased susceptibility of thymocytes to apoptosis in mice lacking AIM, a novel murine macrophage-derived soluble factor belonging to the scavenger receptor cysteine-rich domain superfamily. *J Exp Med* 189:413–422.
14. Kurokawa J, et al. (2010) Macrophage-derived AIM is endocytosed into adipocytes and decreases lipid droplets via inhibition of fatty acid synthase activity. *Cell Metab* 11:479–492.
15. Joseph SB, et al. (2004) LXR-dependent gene expression is important for macrophage survival and the innate immune response. *Cell* 119:299–309.
16. Valledor AF, et al. (2004) Activation of liver X receptors and retinoid X receptors prevents bacterial-induced macrophage apoptosis. *Proc Natl Acad Sci USA* 101: 17813–17818.
17. Gebe JA, et al. (1997) Molecular cloning, mapping to human chromosome 1 q21-q23, and cell binding characteristics of Spalpha, a new member of the scavenger receptor cysteine-rich (SRCR) family of proteins. *J Biol Chem* 272:6151–6158.
18. Kim WK, et al. (2008) Glycoproteomic analysis of plasma from patients with atopic dermatitis: CD5L and ApoE as potential biomarkers. *Exp Mol Med* 40:677–685.
19. Gray J, et al. (2009) A proteomic strategy to identify novel serum biomarkers for liver cirrhosis and hepatocellular cancer in individuals with fatty liver disease. *BMC Cancer* 9:271.
20. Arai S, et al. (2005) A role for the apoptosis inhibitory factor AIM/Spalpha/Api6 in atherosclerosis development. *Cell Metab* 1:201–213.
21. Shi H, et al. (2006) TLR4 links innate immunity and fatty acid-induced insulin resistance. *J Clin Invest* 116:3015–3025.
22. Suganami T, et al. (2007) Role of the Toll-like receptor 4/NF-kappaB pathway in saturated fatty acid-induced inflammatory changes in the interaction between adipocytes and macrophages. *Arterioscler Thromb Vasc Biol* 27:84–91.
23. Poggi M, et al. (2007) C3H/HeJ mice carrying a toll-like receptor 4 mutation are protected against the development of insulin resistance in white adipose tissue in response to a high-fat diet. *Diabetologia* 50:1267–1276.
24. Tsukumo DM, et al. (2007) Loss-of-function mutation in Toll-like receptor 4 prevents diet-induced obesity and insulin resistance. *Diabetes* 56:1986–1998.
25. Davis JE, Gabler NK, Walker-Daniels J, Spurlock ME (2008) Tlr-4 deficiency selectively protects against obesity induced by diets high in saturated fat. *Obesity (Silver Spring)* 16:1248–1255.
26. Kamei N, et al. (2006) Overexpression of monocyte chemoattractant protein-1 in adipose tissues causes macrophage recruitment and insulin resistance. *J Biol Chem* 281:26602–26614.
27. Kanda H, et al. (2006) MCP-1 contributes to macrophage infiltration into adipose tissue, insulin resistance, and hepatic steatosis in obesity. *J Clin Invest* 116:1494–1505.
28. Keophiphath M, Rouault C, Divoux A, Clément K, Lacasa D (2010) CCL5 promotes macrophage recruitment and survival in human adipose tissue. *Arterioscler Thromb Vasc Biol* 30:39–45.
29. Soma MR, Mims MP, Chari MV, Rees D, Morrisett JD (1992) Triglyceride metabolism in 3T3-L1 cells. An in vivo 13C NMR study. *J Biol Chem* 267:11168–11175.
30. Kopp A, et al. (2009) Fatty acids as metabolic mediators in innate immunity. *Eur J Clin Invest* 39:924–933.
31. Schaeffler A, et al. (2009) Fatty acid-induced induction of Toll-like receptor-4/nuclear factor-kappaB pathway in adipocytes links nutritional signalling with innate immunity. *Immunology* 126:233–245.
32. Jenkins KA, Mansell A (2010) TIR-containing adaptors in Toll-like receptor signalling. *Cytokine* 49:237–244.
33. Zechner R, Strauss JG, Haemmerle G, Lass A, Zimmermann R (2005) Lipolysis: Pathway under construction. *Curr Opin Lipidol* 16:333–340.
34. Nishino N, et al. (2008) FSP27 contributes to efficient energy storage in murine white adipocytes by promoting the formation of unilocular lipid droplets. *J Clin Invest* 118: 2693–2696.
35. Schäffler A, Schölmerich J, Salzberger B (2007) Adipose tissue as an immunological organ: Toll-like receptors, C1q/TNFs and CTRPs. *Trends Immunol* 28:393–399.
36. Hoshino K, et al. (1999) Cutting edge: Toll-like receptor 4 (TLR4)-deficient mice are hyporesponsive to lipopolysaccharide: Evidence for TLR4 as the Lps gene product. *J Immunol* 162:3749–3752.

Diabetologia (2012) 55:1745–1754
DOI 10.1007/s00125-012-2521-5

ARTICLE

Control of beta cell function and proliferation in mice stimulated by small-molecule glucokinase activator under various conditions

A. Nakamura · Y. Togashi · K. Orime · K. Sato · J. Shirakawa · M. Ohsugi · N. Kubota · T. Kadowaki · Y. Terauchi

Received: 14 November 2011 / Accepted: 20 February 2012 / Published online: 29 March 2012

Abstract
Aims/hypothesis We investigated changes in the expression of genes involved in beta cell function and proliferation in mouse islets stimulated with glucokinase activator (GKA) in order to elucidate the mechanisms by which GKA stimulates beta cell function and proliferation.
Methods Islets isolated from mice were used to investigate changes in the expression of genes related to beta cell function and proliferation stimulated by GKA. In addition, *Irs2* knockout (*Irs2*$^{-/-}$) mice on a high-fat diet or a high-fat diet containing GKA were used to investigate the effects of GKA on beta cell proliferation in vivo.
Results In wild-type mice, *Irs2* and *Pdx1* expression was increased by GKA. In *Irs2*$^{-/-}$ mice, GKA administration increased the glucose-stimulated secretion of insulin and *Pdx1* expression, but not beta cell proliferation. It was particularly noteworthy that oxidative stress inhibited the upregulation of the *Irs2* and *Pdx1* genes induced by GKA. Moreover, whereas neither GKA alone nor exendin-4 alone upregulated the expression of *Irs2* and *Pdx1* in the islets of *db/db* mice, prior administration of exendin-4 to the mice caused GKA to increase the expression of these genes.
Conclusions/interpretation GKA-stimulated IRS2 production affected beta cell proliferation but not beta cell function. Oxidative stress diminished the effects of GKA on the changes in expression of genes involved in beta cell function and proliferation. A combination of GKA and an incretin-related agent might therefore be effective in therapy.

Keywords Beta cell proliferation · Glucokinase activator · IRS2 · Oxidative stress

Abbreviations

CREB	cAMP-responsive element-binding protein
2-DG	2-Deoxyglucose
GKA	Glucokinase activator
HF	High-fat

Introduction

Glucokinase is the predominant enzyme involved in glucose phosphorylation in beta cells and hepatocytes, and it plays an important role as a glucose sensor in beta cells and as a regulator of glucose metabolism in the liver [1, 2]. In addition, glucokinase plays a pivotal role in regulating not only beta cell function, but also beta cell mass [3, 4].

Since the report by Grimsby et al in 2003 [5], several glucokinase activators (GKAs) have been developed, and these have been shown to lower blood glucose in several animal models of type 2 diabetes [5–12]. In a study of beta cell function, it was reported that a GKA stimulated insulin secretion in a Ca^{2+}-dependent manner in rodent islets and MIN6 cells [13], and we and others have reported that GKAs promoted beta cell proliferation and increased production of IRS2 [11, 14], which is critically required for beta

A. Nakamura · Y. Togashi · K. Orime · K. Sato · J. Shirakawa · Y. Terauchi (✉)
Department of Endocrinology and Metabolism, Graduate School of Medicine, Yokohama City University, 3-9 Fukuura, Kanazawa-ku, Yokohama 236-0004, Japan
e-mail: terauchi-tky@umin.ac.jp

M. Ohsugi · N. Kubota · T. Kadowaki
Department of Diabetes and Metabolic Diseases, Graduate School of Medicine, University of Tokyo, Tokyo, Japan

cell growth and survival [3, 15–17]. However, the exact mechanisms by which GKAs stimulate beta cell function and proliferation are largely unknown.

Single- and multiple-dose placebo-controlled studies in human have recently reported that GKAs reduce the fasting and postprandial glucose levels of patients with type 2 diabetes and of healthy adults [18, 19]. Notably, however, another GKA, MK-0941, led to improvements in glycaemic control that were not sustained [20]. Therefore, a better understanding of the underlying mechanism is needed to determine whether glucokinase activation with GKAs is a feasible treatment goal for individuals with type 2 diabetes.

In the present study, we first investigated changes in the expression of genes involved in beta cell function and proliferation in mouse islets stimulated with GKA in order to elucidate the mechanisms by which GKA stimulated beta cell function and proliferation. We then explored therapeutic strategies by which GKA might work more effectively.

Methods

Chemicals A GKA (3-[(1*S*)-2-hydroxy-1-methylethoxy]-5-[4-(methylsulfonyl)phenoxy]-*N*-1,3-thiazol-2-yl benzamide) was prepared by Tsukuba Research Institute, Banyu Pharmaceutical, Tokyo, Japan, as previously described [21].

Animals *Irs2*$^{-/-}$ mice were generated as described elsewhere [16] and were then backcrossed with C57Bl/6J mice more than nine times. Both wild-type and *Irs2*$^{-/-}$ male mice were fed standard chow until 8 weeks of age, when they were given free access to either the standard chow, a high-fat (HF) diet, or an HF diet containing GKA. To evaluate the effect of GKA on glucose metabolism in vivo more thoroughly, wild-type and *Irs2*$^{-/-}$ mice were divided into four groups: wild-type mice fed the HF diet, wild-type mice fed the HF diet containing 0.04% GKA, *Irs2*$^{-/-}$ mice fed the HF diet, and *Irs2*$^{-/-}$ mice fed the HF diet containing 0.04% GKA. Five-week-old male *db/db* mice were purchased from Charles River Laboratories Japan (Yokohama, Japan). When they were 6 weeks of age, they were intraperitoneally injected with normal saline or exendin-4 (100 μg/kg; Sigma-Aldrich, Tokyo, Japan) once daily for 2 weeks. The mice were housed under a 12-h light/dark cycle. The animals were maintained in accordance with standard animal care procedures based on the institutional guidelines.

Diet protocol Standard chow (MF; Oriental Yeast, Tokyo, Japan) and an HF diet (High Fat Diet 32; Clea Japan, Tokyo, Japan) were used. GKA was administrated in the form of a 0.04% (wt/wt) admixture to the HF diet as previously described [11].

Glucose tolerance test Mice were fasted for 4 h before the study, and then orally loaded with a 1.5 mg/g body weight dose of glucose. Blood glucose was measured with a Glutest Neo portable glucose meter (Sanwa Chemical, Nagoya, Japan).

Immunohistochemical analysis to estimate beta cell mass Isolated pancreases were immersion-fixed in 10% formalin at 4°C overnight. Tissue was then routinely processed for paraffin embedding, and 5 μm sections mounted on glass slides were immunostained with rabbit anti-human insulin (diluted 1:1,000) antibody (Santa Cruz Biotechnology, Santa Cruz, CA, USA). The area of the beta cells was calculated with WinROOF software (Mitani, Tokyo, Japan) as described elsewhere [3]. Approximately 100 islets per mouse were counted in each group.

Analysis of BrdU incorporation Wild-type and *Irs2*$^{-/-}$ mice on the HF diet for 10 weeks were divided into two groups: an HF diet group, and a group given 0.04% GKA mixed into the HF diet. After 3 days, the mice were intraperitoneally injected with BrdU (Nacalai Tesque, Kyoto, Japan), and the pancreases were removed 6 h later. Immunohistochemical detection of BrdU was performed with a commercial kit (BD Biosciences, Franklin Lakes, NJ, USA). Approximately 100 islets per mouse were counted in each group.

Islet isolation Islets were isolated by using liberase RI (Roche Diagnostics, Indianapolis, IN, USA) or collagenase XI (Sigma-Aldrich, St Louis, MO, USA) according to the manufacturer's instructions, as described elsewhere [3, 11].

Analysis of insulin secretion Insulin secretion was measured after culturing islets overnight in RPMI 1640 medium containing 11 mmol/l glucose supplemented with 10% fetal calf serum, 100 U/ml penicillin and 100 μg/ml streptomycin (Sigma-Aldrich, St Louis, MO, USA). Ten islets were incubated at 37°C for 1.5 h in Krebs–Ringer bicarbonate buffer containing 5.6 or 22 mmol/l glucose in the absence or presence of GKA. The insulin concentration of the assay buffer was measured with an insulin ELISA kit (Morinaga, Yokohama, Japan).

Real-time quantitative PCR Total RNA was isolated with the RNeasy Mini Kit (Qiagen, Hilden, Germany) and used as the starting material for complementary DNA (cDNA) preparation. cDNA was synthesised by using TaqMan Reverse Transcription Reagents (Applied Biosystems, Foster City, CA, USA), and TaqMan quantitative PCR was performed with the ABI Prism 7500 PCR instrument (Applied Biosystems).

Western blot analysis The anti-phospho [Ser133] cAMP-responsive element-binding protein (CREB), total CREB,

and cyclin D2 antibody were purchased from Cell Signaling Technology (Beverly, MA, USA). Anti-IRS2 antibody was purchased from Upstate (Temecula, CA, USA). Protein was prepared from more than 100 islets pooled from several mice in the same group, and 20 μg of protein samples were applied to the gel. Protein bands were visualised with the ECL Plus Western Blotting Detection System (GE Healthcare, Amersham, UK).

Statistical analysis Results are expressed as mean ± SE (*n*). Differences between two groups were analysed for statistical significance by Student's *t* test. Individual comparisons between more than two groups were assessed by the post hoc Fisher's PLSD test. A p value <0.05 was considered statistically significant.

Results

Mechanism of the upregulation of Irs2 expression in response to GKA-induced glucokinase activation Because we had hypothesised that glucose metabolism via glucokinase would increase the phosphorylation of CREB and the production of IRS2 [3, 22], we investigated whether the GKA was able to stimulate the phosphorylation of CREB. Ser133 phosphorylation of CREB was significantly increased at 22 mmol/l glucose in comparison with 5.6 mmol/l glucose, and the GKA stimulated the Ser133 phosphorylation of CREB in the isolated islets of wild-type mice at 5.6 mmol/l glucose (Fig. 1a). The phosphorylation of CREB paralleled the upregulation of IRS2 production.

As it has been reported that glucose treatment of isolated islets potently increases *Irs2* expression via glucose metabolism and Ca^{2+} influx [23], we examined changes in *Irs2* mRNA levels in response to GKA administration or high-glucose stimulation under several conditions to identify the mechanism of *Irs2* upregulation. First, we evaluated *Irs2* mRNA expression in response to the GKA and sulfonylureas. Real-time quantitative PCR showed that *Irs2* mRNA was significantly increased with 22 mmol/l glucose in comparison with 5.6 mmol/l glucose (Fig. 1c). The GKA also significantly increased *Irs2* mRNA with 5.6 mmol/l glucose, but neither gliclazide nor glibenclamide upregulated the *Irs2* mRNA level (Fig. 1c).

Next, we used the non-metabolisable analogue of glucose, 2-deoxyglucose (2-DG), to investigate whether glucose metabolism was required for GKA-stimulated *Irs2* expression. When glucose was replaced by 2-DG, the *Irs2* mRNA levels did not increase in response to the GKA or a stimulatory concentration of 2-DG (22 mmol/l; Fig. 1d), indicating that glucose metabolism is necessary for GKA-induced *Irs2* expression to occur in islet beta cells.

We also conducted experiments using an L-type calcium channel blocker (nifedipine) and calcineurin inhibitor

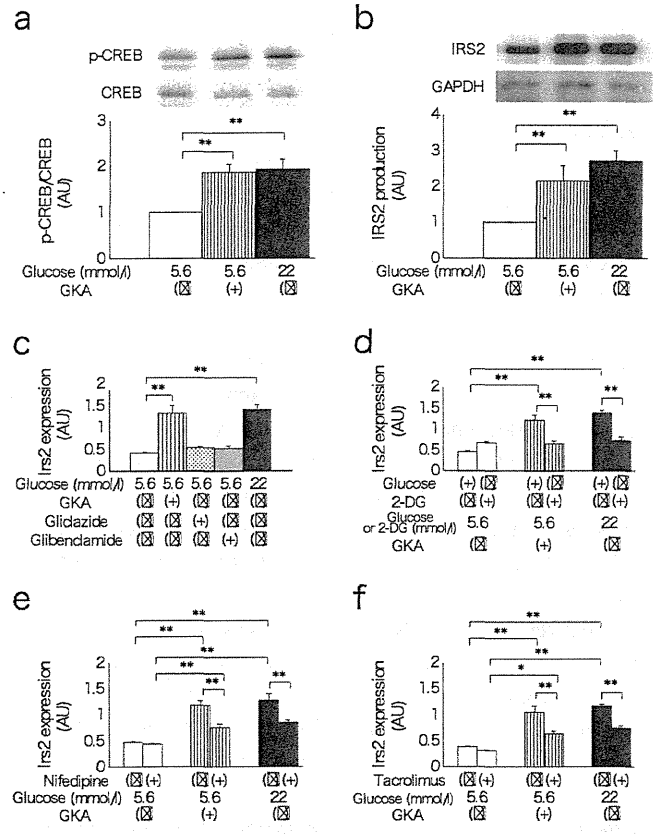

Fig. 1 Effect of GKA on upregulation of *Irs2* expression. **a** Western blot assay of phospho [Ser133] CREB (p-CREB) and total CREB levels in islets. **b** Production of IRS2 in islets. Islets from wild-type mice were stimulated with 5.6 mmol/l glucose in the absence or presence of 6 μmol/l GKA or with 22 mmol/l glucose alone. Equal amounts of lysates were blotted with the p-CREB, total CREB, IRS2 and GAPDH antibody. Expression levels were quantified. The intensity of p-CREB was normalised to total CREB expression, and the intensity of IRS2 was normalised to GAPDH expression (white bar, 5.6 mmol/l glucose; hatched bar, 5.6 mmol/l glucose plus GKA; black bar, 22 mmol/l glucose) (*n*=5). **c**–**f** Effects of (**c**) sulfonylureas (10 μmol/l gliclazide and 1 nmol/l glibenclamide), (**d**) 2-deoxyglucose (DG), (**e**) 50 μmol/l nifedipine, and (**f**) 10 μmol/l tacrolimus on *Irs2* expression. The *Irs2* and beta-actin (control) mRNA levels of isolated islets in wild-type mice were measured by real-time quantitative PCR. Data have been normalised to beta-actin expression (white bars, 5.6 mmol/l glucose; hatched bars, 5.6 mmol/l glucose plus GKA; dotted bars, 5.6 mmol/l glucose plus gliclazide; grey bar, 5.6 mmol/l glucose plus glibenclamide; black bars, 22 mmol/l glucose) (*n*=3 or 4). Values are mean ± SE. *p<0.05; **p<0.01

(tacrolimus). The results showed that both nifedipine (50 μM) and tacrolimus (10 μM) significantly inhibited the upregulation of *Irs2* mRNA levels induced by GKA administration or high-glucose stimulation, although the *Irs2* mRNA levels remained slightly but significantly increased (Fig. 1e, f). These results indicated that the GKA-induced *Irs2* upregulation in islets is at least partly Ca^{2+}-dependent and mediated by calcineurin.

Effect of the GKA on changes in gene expression in isolated islets Next, we investigated changes in the expression levels of genes involved in beta cell function and proliferation in the

islets of wild-type mice in the absence or presence of the GKA. *Pdx1* is the major regulator of glucose-stimulated insulin gene transcription, and its mRNA level was significantly increased at 22 mmol/l glucose in comparison with 5.6 mmol/l glucose; in addition, the GKA stimulated *Pdx1* mRNA production with 5.6 mmol/l glucose in the isolated islets of wild-type mice (Fig. 2a). The increased *Pdx1* levels paralleled the upregulation of *Glut2*, *Gck*, *Ins1* and *Ins2* expression (Fig. 2a). Gliclazide, however, failed to increase the expression levels of these (Fig. 2b). These results indicated that the GKA improved beta cell function at the transcriptional level.

As the results of a DNA microarray analysis we previously reported showed decreased expression of *Pdpk1* and *Ccnd2* in $Gck^{+/-}$ mice in comparison with wild-type mice on the HF diet [3], we investigated the expression levels of these and other cell-cycle-related genes in the present study. GKA and high-glucose stimulation significantly increased *Pdpk1*, *Ccnd1*, *Ccnd2* and *Ccnd3* mRNA expression, but the expression of *Cdk4* and p27 was unaltered (Fig. 2c). Cyclin D2 protein levels were also increased by the GKA and high-glucose stimulation (Fig. 2d). These results suggested an involvement of cell cycle signalling, such as by cyclin D2, in GKA-stimulated beta cell proliferation.

Effect of the GKA on glucose metabolism and beta cell mass in $Irs2^{\square/\square}$ *mice* We used $Irs2^{-/-}$ mice to determine whether IRS2 was required for the therapeutic effects of the GKA, and divided the animals into four groups: wild-type mice fed the HF diet (WT group), wild-type mice fed a diet containing 0.04 % GKA mixed into the HF diet (WT+GKA group), $Irs2^{-/-}$ mice fed the HF diet (IRS2 group), and $Irs2^{-/-}$ mice fed 0.04% GKA mixed into the HF diet (IRS2+GKA group).

There were no significant differences in body weight between mice receiving and mice not receiving GKA in both the wild-type and $Irs2^{-/-}$ groups (Fig. 3a). The blood glucose level decreased shortly after consuming the HF diet containing the GKA. The blood glucose level of the WT+GKA group was significantly lower than that of the WT group, and the blood glucose level of the IRS2+GKA group was significantly lower than that of the IRS2 group (Fig. 3b). We also performed an OGTT on these four groups of mice (Fig. 3c). The area under the curve (0–120 min) of the blood glucose levels during the OGTT was significantly decreased in both the wild-type and $Irs2^{-/-}$ mice that received the GKA compared with the mice that did not receive the GKA (Fig. 3d). Thus, GKA demonstrated glucose-lowering efficacy without affecting body weight in both the wild-type and $Irs2^{-/-}$ mice on the HF diet.

Next, to investigate the effect of GKA on beta cell mass, we measured the beta cell mass of the mice. Histological analysis revealed that the area of the beta cells was significantly increased in the wild-type mice in comparison with the $Irs2^{-/-}$ mice (Fig. 3e), consistent with our previous report [3], but no further increase was observed in response to administering GKA to either genotype of mouse (Fig. 3e).

As we previously reported [11], the absence of any effect of the GKA on the beta cell mass of the $Irs2^{-/-}$ mice may be attributable to a suppression of beta cell proliferation due to

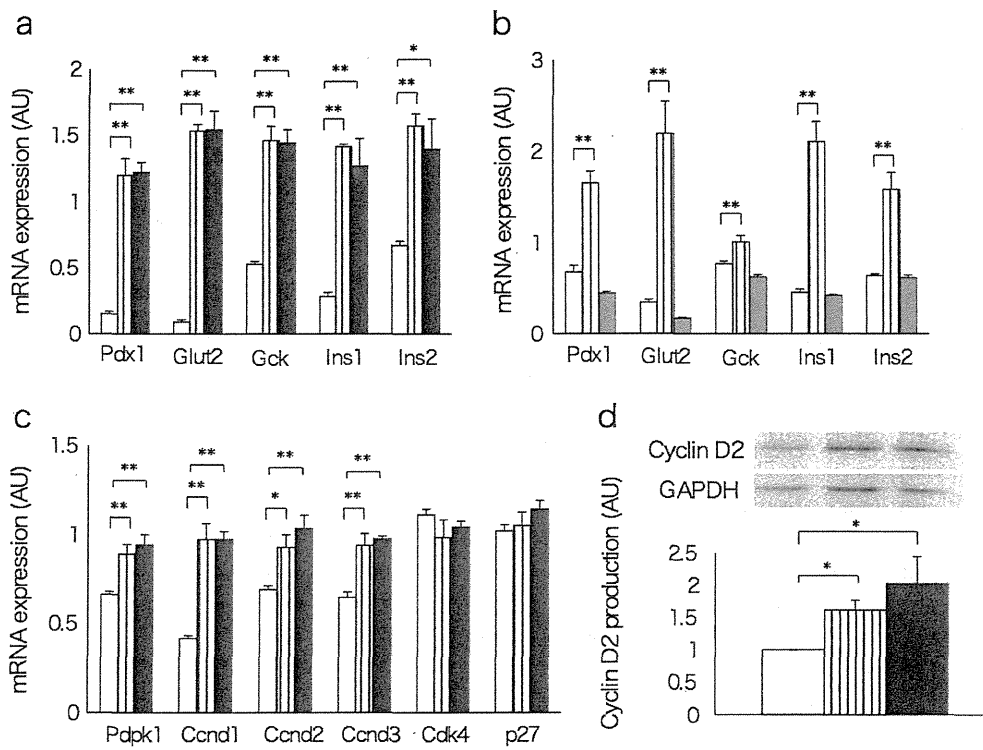

Fig. 2 Changes in gene expression levels in islets stimulated with GKA. a□c The mRNA levels of (**a, b**) *Pdx1*, *Glut2*, *Gck*, *Ins1* and *Ins2*, and of (**c**) *Pdpk1*, *Ccnd1*, *Ccnd2*, *Ccnd3*, *Cdk4* and *p27* in islets measured by real-time quantitative PCR. Data have been normalised to beta-actin expression. **d** Western blot assay of cyclin D2 levels in islets. Equal amounts of lysates were blotted with the cyclin D2 antibody and GAPDH antibody. Protein levels were quantified, and the cyclin D2 data have been normalised to GAPDH expression (white bars, 5.6 mmol/l glucose; hatched bars, 5.6 mmol/l glucose plus GKA; grey bars, 5.6 mmol/l glucose plus gliclazide; black bars, 22 mmol/l glucose) (n 3–5). Values are mean ± SE. *$p<0.05$; **$p<0.01$

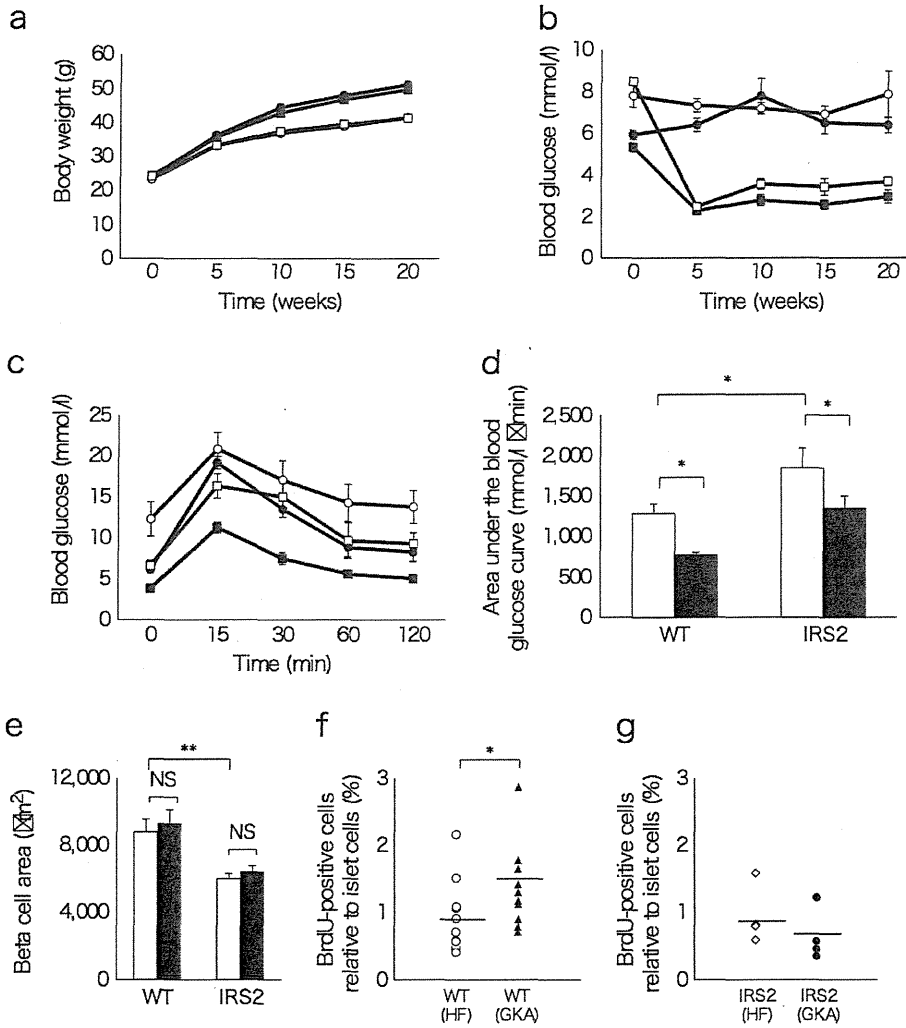

Fig. 3 Impact of GKA on glucose metabolism and on beta cell mass and proliferation in *Irs2*$^{-/-}$ mice. **a, b** Changes in (**a**) body weight and (**b**) fed blood glucose level. Wild-type mice on the HF diet (WT; black circles), wild-type mice fed the 0.04% GKA HF diet (WT+GKA; black squares), *Irs2*$^{-/-}$ mice fed the HF diet (IRS2; white circles) and *Irs2*$^{-/-}$ mice fed the 0.04% GKA HF diet (IRS2+GKA; white squares) (*n* 8). **c** Blood glucose levels during the OGTT in the WT group (black circles), WT+GKA group (black squares), IRS2 group (white circles) and IRS2+GKA group (white squares) (*n* 7 or 8). **d** Area under the curve of the glucose excursion during the OGTT in the mice on the HF diet (white bars) or on the 0.04% GKA HF diet (black bars) (*n* 7 or 8). **e** Quantification of beta cell mass. Histological analysis of pancreatic islets from the mice on the HF diet (white bars) and the 0.04% GKA HF diet (black bars) (*n* 4 or 5). **f, g** Replication rates, assessed by BrdU incorporation after administration of GKA for 3 days, were determined in (**f**) WT mice and (**g**) *Irs2*$^{-/-}$ mice after 10 weeks on the HF diet. Results are shown as vertical scatter plots for the wild-type mice without GKA (white circles) and with GKA (black triangles), and *Irs2*$^{-/-}$ mice without GKA (white diamonds) and with GKA (black circles) (*n* 4–11). Values are mean ± SE. **p*<0.05; ***p*<0.01

the chronic reduction in ambient blood glucose levels induced by the GKA treatment rather than to the deficiency of IRS2. To investigate this possibility, we evaluated beta cell proliferation after administering the GKA on three consecutive days to mice fed the HF diet for 10 weeks; the results showed a significant decrease in the fed blood glucose level of both the wild-type and *Irs2*$^{-/-}$ mice shortly after administration of the GKA (data not shown). The BrdU incorporation ratio was significantly increased in the wild-type mice given the GKA for 3 days in comparison with the wild-type mice not given the GKA; this was not, however, seen in the *Irs2*$^{-/-}$ mice (Fig. 3f, g). These results support the concept that IRS2 could have an effect on beta cell proliferation stimulated by a GKA in vivo.

Effect of the GKA on the beta cell function of Irs2$^{-/-}$ *mice* To investigate the effect of the GKA on beta cell function ex vivo, we evaluated glucose-stimulated insulin secretion by the islets of *Irs2*$^{-/-}$ mice. Insulin secretion by *Irs2*$^{-/-}$ islets in response to 5.6 mmol/l glucose was significantly increased in the presence of GKA (Fig. 4a). The increase in insulin secretion in response to the application of 22 mmol/l glucose was less evident, suggesting that the secretion had peaked. These findings indicated that the GKA

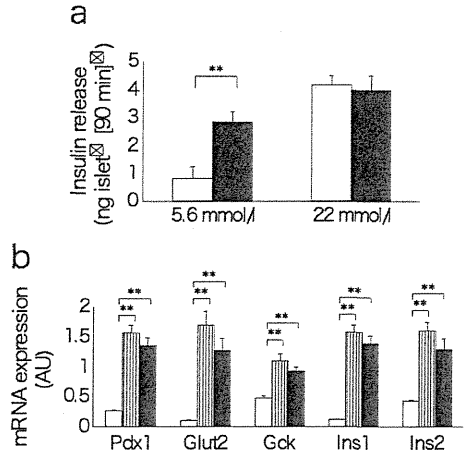

Fig. 4 Impact of GKA on glucose-stimulated insulin secretion ex vivo and changes in expression of genes involved in beta cell function in islets isolated from *Irs2*$^{-/-}$ mice. **a** Insulin secretion was measured with 5.6 mmol/l or 22 mmol/l glucose in the absence or presence of GKA. Results are shown as nanograms of insulin islet^{-1} 90 min^{-1} (n 7). Values are mean ± SE of data obtained from the analysis of islets isolated from *Irs2*$^{-/-}$ mice treated with vehicle (white bars) or 6 μmol/l GKA (black bars). **b** mRNA levels of *Pdx1*, *Glut2*, *Gck*, *Ins1* and *Ins2* in islets from *Irs2*$^{-/-}$ mice were measured by real-time quantitative PCR. Data have been normalised to beta-actin expression (white bars, 5.6 mmol/l glucose; hatched bars, 5.6 mmol/l glucose plus GKA; black bars, 22 mmol/l glucose) (n 3 or 4). Values are mean ± SE. **p<0.01

had stimulated glucose-stimulated insulin secretion by increasing glucose sensitivity without altering maximum insulin secretion by the *Irs2*$^{-/-}$ islets, which is consistent with our previous findings in wild-type and *Gck*$^{+/-}$ islet cells [11].

Next, we investigated whether the GKA affected the expression of genes involved in beta cell function in islets isolated from *Irs2*$^{-/-}$ mice. *Pdx1* mRNA significantly increased with 22 mmol/l glucose in comparison with 5.6 mmol/l glucose, and the GKA stimulated *Pdx1* mRNA expression at 5.6 mmol/l glucose in the isolated islets of *Irs2*$^{-/-}$ mice (Fig. 4b). In addition, there were no differences in *Pdx1* expression 5.6 mmol/l glucose in wild-type and *Irs2*$^{-/-}$ mice, and *Pdx1* expression was significantly increased with 22 mmol/l glucose or by the GKA in both genotypes of mouse to the same degree (data not shown). The increased *Pdx1* expression also paralleled the upregulation of *Glut2*, *Gck*, *Ins1* and *Ins2* levels (Fig. 4b). These results indicated that GKA enhanced beta cell function at the transcriptional level independently of IRS2.

Effect of oxidative stress on GKA-induced Irs2 and Pdx1 expression Exposure to exogenous H_2O_2 is known to reduce glucose-induced insulin secretion by impairing mitochondrial metabolism in beta cells [24]. This knowledge prompted us to evaluate the effect of oxidative stress on GKA-induced changes in the expression of genes related to beta cell function and proliferation. We investigated GKA-stimulated *Irs2* and *Pdx1* expression after H_2O_2 preconditioning. H_2O_2 significantly inhibited the upregulation of *Irs2* and *Pdx1* induced by GKA (Fig. 5a, b), and the inhibition was prevented by prior administration of alpha-tocopherol plus ascorbate (Fig. 5c, d). These results indicated that oxidative stress prevented GKA affecting the expression of genes related to beta cell function and proliferation.

Effect of GKA on Irs2 and Pdx1 expression in db/db mice Based on the above results, we next evaluated the effect of GKA on *Irs2* and *Pdx1* expression in *db/db* mice, a well-known model of type 2 diabetes accompanied by obesity and characterised by increased insulin resistance and severe damage to the pancreatic beta cells. The levels of gene expression for the reduced-form NADPH oxidase complex were coordinately elevated in islets isolated from *db/db* mice in comparison with islets isolated from wild-type mice (Fig. 6a–c), and thus the islets from the *db/db* mice could be exposed to oxidative stress. In contrast to the islets isolated from the wild-type mice, GKA failed to increase *Irs2* and *Pdx1* expression in islets isolated from the *db/db*

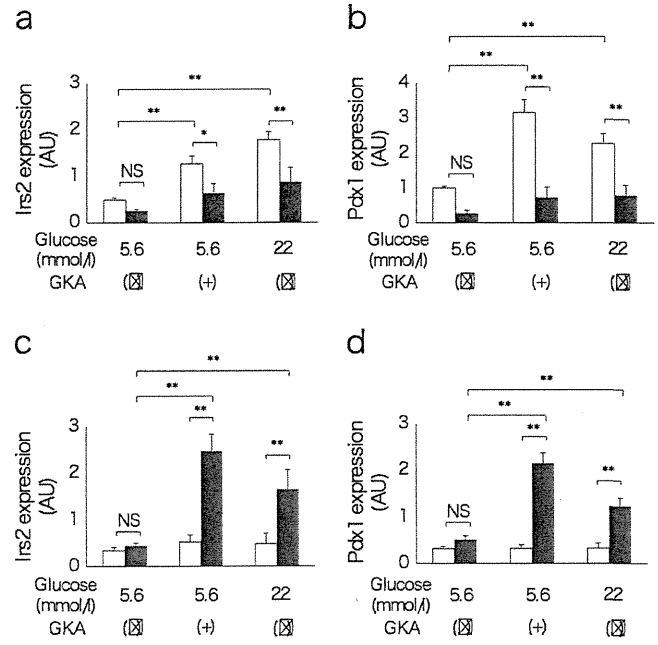

Fig. 5 Effect of GKA on changes in *Irs2* and *Pdx1* expression levels under oxidative stress. **a, b** mRNA levels of (**a**) *Irs2* and (**b**) *Pdx1* in islets from wild-type mice after H_2O_2 preconditioning were measured by real-time quantitative PCR. Isolated islets were incubated overnight with RPMI1640 medium containing 5.6 mmol/l glucose with or without 50 μmol/l H_2O_2 (white bars, absence of H_2O_2; black bars, presence of H_2O_2). **c, d** Effect of antioxidant treatment on GKA-stimulated *Irs2* (**c**) and *Pdx1* (**d**) expression. Isolated islets were incubated overnight with RPMI1640 medium containing 5.6 mmol/l glucose and 50 μmol/l H_2O_2 with or without alpha-tocopherol plus ascorbate (white bars, absence of alpha-tocopherol plus ascorbate; black bars, presence of alpha-tocopherol plus ascorbate). Data have been normalised to beta-actin expression (n 4). Values are mean ± SE. *p<0.05; **p<0.01

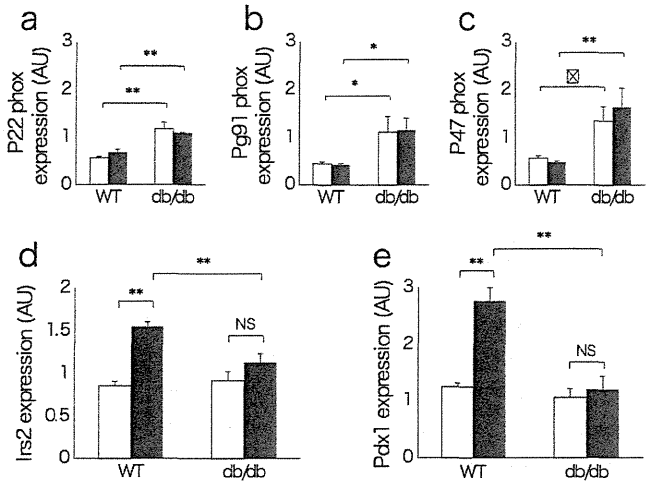

Fig. 6 Changes in expression of genes in isolated islets of *db/db* mice stimulated with GKA. mRNA levels of (**a**) *P22phox* (also known as *Cyba*), (**b**) *Pg91phox* (also known as *Cybb*), (**c**) *P47phox* (also known as *Ncf1*), (**d**) *Irs2* and (**e**) *Pdx1* in islets from 8-week-old wild-type and *db/db* mice were measured by real-time quantitative PCR. Data have been normalised to beta-actin expression (white bars, absence of GKA; black bars, presence of GKA) (n 4). Values are mean ± SE. *p<0.05; **p<0.01; †p 0.05

mice (Fig. 6d, e). These results showed that the effects of GKA on the expression of genes related to beta cell function and proliferation were diminished in the islets from the *db/db* mice.

Effect of exendin-4 on GKA-stimulated Irs2 and Pdx1 expression in db/db mice In order to increase *Irs2* and *Pdx1* expression stimulated by GKA in *db/db* mice, exendin-4 was intraperitoneally injected into *db/db* mice for 2 weeks before isolating the islets. Exendin-4 decreased blood glucose levels without affecting body weight (Fig. 7a, b). Remarkably, GKA was able to upregulate *Irs2* and *Pdx1* expression in the islets of *db/db* mice after prior administration of exendin-4 (Fig. 7c, d). It is noteworthy that exendin-4 alone was insufficient to upregulate these molecules. However, under our experimental conditions, the expression levels of genes for the reduced-form NADPH oxidase complex were unchanged (Fig. 7e–g).

Discussion

The results of the present study yielded three new findings. First, glucokinase activation by the GKA, a glucose-like activator of beta cell metabolism, increased IRS2 production; in addition, GKA-stimulated IRS2 production was able to affect beta cell proliferation, but not beta cell function. Second, the effects of the GKA on the expression of genes involved in beta cell function and proliferation were diminished in islets exposed to exogenous H_2O_2 and in those from *db/db* mice. Third, a combination of GKA and an incretin-related agent was effective in upregulating *Irs2* and *Pdx1* expression in these islets.

GKA increased the phosphorylation of CREB and IRS2 production (Fig. 1a, b), and 2-DG failed to increase *Irs2* expression by GKA (Fig. 1d). Both nifedipine and tacrolimus partly, but significantly, inhibited upregulation of *Irs2* expression by GKA (Fig. 1e, f). Taken together with the previous study [25], these results suggest that GKA increased CREB phosphorylation and *Irs2* expression in islets via glucose metabolism, Ca^{2+} influx and, in part, a Ca^{2+}–calcineurin pathway. In contrast, *Irs2* expression was not increased by either of the sulfonylureas. Sulfonylureas are known to close ATP-sensitive potassium channels regardless of glucose metabolism, and their closure results in membrane depolarisation, an influx of Ca^{2+} through voltage-dependent Ca^{2+} channels, and an increase in cytosolic free Ca^{2+} concentration, thereby triggering insulin secretion [26]. If that is true, why did the sulfonylureas fail to increase *Irs2* expression despite being able to increase the Ca^{2+} influx? One possible explanation is that the glucose flux per se may also be needed to increase *Irs2* expression and lead to beta cell proliferation [3, 22], since the sulfonylurea glibenclamide is unable to increase beta cell

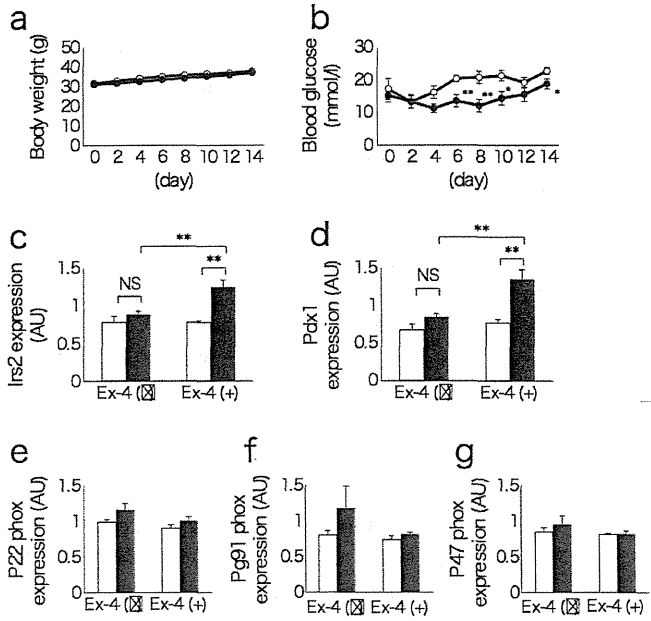

Fig. 7 Effect of a combination of exendin-4 and GKA on *Irs2* and *Pdx1* expression in *db/db* mice. **a, b** Changes in (**a**) body weight and (**b**) fed blood glucose levels of *db/db* mice injected or not injected with exendin-4 (Ex-4) for 2 weeks (white circles, not injected with Ex-4; black circles, injected with Ex-4) (n 8). The mRNA levels of (**c**) *Irs2*, (**d**) *Pdx1*, (**e**) *P22phox* (also known as *Cyba*), (**f**) *Pg91phox* (also known as *Cybb*) and (**g**) *P47phox* (also known as *Ncf1*) in islets from *db/db* mice were measured by real-time quantitative PCR. Data have been normalised to beta-actin expression (white bars, absence of GKA; black bars, presence of GKA) (n 5). Values are mean ± SE. *p<0.05; **p<0.01

proliferation in wild-type mice [27]. We therefore hypothesised that both glucose metabolism and Ca^{2+} influx are required to increase *Irs2* expression and lead to beta cell proliferation. This hypothesis is supported by a report that glibenclamide increases beta cell proliferation in the presence of an increased glucose flux [27].

The *Pdx1* expression level has been reported to be severely reduced in the beta cells of $Irs2^{-/-}$ mice with a certain genetic background [28], suggesting that IRS2 may directly regulate the expression and function of *Pdx1*, and thereby maintain beta cell growth and function. However, GKA upregulated the expression of *Pdx1* and several downstream genes, *Glut2*, *Gck*, *Ins1* and *Ins2*, in the isolated islets of $Irs2^{-/-}$ mice with a C57BL/6 background (Fig. 4b). In regard to this point, Suzuki et al reported finding that *Pdx1* expression in $Irs2^{-/-}$ mice is regulated in a strain-dependent manner [29]. *Pdx1* expression was not downregulated in our $Irs2^{-/-}$ murine beta cells that had a C57BL/6J background [29]. We therefore assume that GKA increased glucose-stimulated insulin gene transcription independently of IRS2. Since Kushner et al reported that transgenic overexpression of *Pdx1* restored beta cell mass in $Irs2^{-/-}$ mice [28], *Pdx1* may play a role in regulating beta cell mass. Nevertheless, because a haploinsufficiency of *Pdx1* led to impaired beta cell function, but not to decreased beta cell mass [30], and because beta cell mass was smaller in our $Irs2^{-/-}$ mice than in wild-type mice despite the *Pdx1* expression level being maintained [29], two different pathways are involved in the stimulation of beta cell function and proliferation by a GKA.

The results of our study have clinical implications. As stated above, MK-0941 lacked durability in glycaemic control [20]. In these patients, disease-related characteristics were a mean baseline HbA_{1c} of 9.0 % (75 mmol/mol), a mean duration of diabetes of 12 years, and a mean insulin glargine (A21Gly,B31Arg,B32Arg human insulin) dose of 45 U/day. These data suggest that the insulin secretion or the beta cells themselves were severely impaired. From these clinical trials, it is possible that a pancreatic effect of GKAs could not be expected when pancreatic beta cells have been impaired. It is well known that the level of 8-hydroxydeoxyguanosine, a marker of oxidative stress, is increased in diabetic patients and independently associated with mean HbA_{1c} [31]; in addition, increased oxidative stress influences beta cell function, and antioxidant treatment can exert beneficial effects in diabetes, with a preservation of beta cell function [32]. We therefore investigated the effect of oxidative stress on GKA-induced changes in the expression of genes involved in beta cell function and proliferation. As expected, the results showed that oxidative stress inhibited the upregulation of *Irs2* and *Pdx1* in response to GKA, although the inhibition was prevented by prior administration of an antioxidant (Fig. 5). Moreover, the levels of these molecules were not increased by GKA in islets isolated from *db/db* mice (Fig. 6).

Although our findings could support the observation that GKA is ineffective in patients with type 2 diabetes whose pancreatic beta cells have been impaired, there are some limitations to our study. First, with regard to the experiment with exogenous H_2O_2, we could not rule out the possibility that the absence of increasing *Irs2* and *Pdx1* expression after H_2O_2 preconditioning was caused by not only impaired mitochondrial function, but also an impaired biological response of these islets independently of GKA activity. It is also possible that *Gck* expression level might have an effect on the inhibition of upregulation of *Irs2* and *Pdx1* induced by 5.6 mmol/l glucose plus GKA. Second, with regard to the experiment with the *db/db* mice, GKA compounds act to reduce glucose levels in the *db/db* mouse model, as shown with MK-0941 and other agents [8, 33]. The background of the *db/db* mice or the difference in compounds could influence the effect of GKAs. Thus, greater study of the glucose-lowering effect of the GKA in *db/db* mice is needed.

In the present study, we also explored the therapeutic strategy by which GKA worked more effectively in these impaired beta cells. Based on the results of this study, we propose that GKA should be used before pancreatic beta cell failure. First, GKA should be used earlier, as diabetes is progressing, since beta cell failure has already progressed before the diagnosis of diabetes is made [34, 35]. The efficacy of long-term GKA therapy should be assessed in patients with mild type 2 diabetes or impaired glucose tolerance. Second, GKA should be used in combination with incretin therapy in case GKA monotherapy is ineffective. The results of our study indicated that GKA stimulated *Irs2* and *Pdx1* expression in the islets of *db/db* mice when exendin-4 had been administered in advance (Fig. 7). This finding suggested that combination therapy consisting of a GKA and an incretin may be useful for patients with type 2 diabetes. We previously speculated that the increase in *Irs2* expression in the islets of *db/db* mice in response to the combination of these drugs was due to the reduction of oxidative stress or the additive effect of Ca^{2+} influx via glucose signalling and cAMP signalling through the human glucagon-like peptide-1 receptors [22]. However, the levels of expression of the genes for the reduced-form NADPH oxidase complex were unchanged by prior administration of exendin-4 under our experimental conditions (Fig. 7e–g). Since *Irs2* expression was not increased by exendin-4 alone (Fig. 7c), we assume that exendin-4 amplifies GKA-stimulated calcium signalling rather than imposing it. Further study is needed to test the combination in vivo on glycaemic control and the resultant changes in pancreatic gene transcription.

In conclusion, GKA-stimulated IRS2 production affected beta cell proliferation, but not beta cell function. Oxidative

stress was able to prohibit the ability of GKA to change the expression of genes involved in beta cell function and proliferation. A combination of GKA and an incretin-related agent might be effective here. These findings suggest that the GKAs should have outstanding potential for the treatment of diabetes and related disorders.

Acknowledgements We thank M. Kaji and E. Sakamoto (Yokohama City University, Yokohama, Japan) for their excellent technical assistance and animal care.

Funding This work was supported in part by a Grant-in-Aid for Scientific Research (B) 19390251 and (B) 21390282 from the Ministry of Education, Culture, Sports, Science and Technology (MEXT) of Japan, a Medical Award from the Japan Medical Association, a Grant-in-Aid from the Japan Diabetes Foundation, a Grant-in-Aid from Novo Nordisk Pharma, a Grant-in-Aid from the Suzuken Memorial Foundation, a Grant-in-Aid from the Naito Foundation, a Grant-in-Aid from the Yamaguchi Endocrine Research Foundation, a Grant-in-Aid from the Uehara Memorial Foundation (to Y. Terauchi) as well as a Grant-in-Aid for Young Scientists (Start-up) 21890213 and (B) 23791040 from the MEXT of Japan, a Grant-in-Aid from Yokohama General Promotion Foundation, and a Grant-in-Aid from Japan Diabetes Foundation (to A. Nakamura).

Duality of interest The authors declare that there is no duality of interest associated with this manuscript.

Contribution statement All authors conceived and designed the study, and participated in the analysis and interpretation of the data. AN drafted the manuscript and all other authors revised it critically for intellectual content. All authors approved the final version of the paper.

References

1. Matschinsky FM (1996) Banting Lecture 1995. A lesson in metabolic regulation inspired by the glucokinase glucose sensor paradigm. Diabetes 45:223–241
2. Matschinsky FM, Glaser B, Magnuson MA (1998) Pancreatic beta-cell glucokinase: closing the gap between theoretical concepts and experimental realities. Diabetes 47:307–315
3. Terauchi Y, Takamoto I, Kubota N et al (2007) Glucokinase and IRS-2 are required for compensatory beta cell hyperplasia in response to high-fat diet-induced insulin resistance. J Clin Invest 117:246–257
4. Kassem S, Bhandari S, Rodríguez-Bada P et al (2010) Large islets, beta-cell proliferation, and a glucokinase mutation. N Engl J Med 362:1348–1350
5. Grimsby J, Sarabu R, Corbett WL et al (2003) Allosteric activators of glucokinase: potential role in diabetes therapy. Science 301:370–373
6. Efanov AM, Barrett DG, Brenner MB et al (2005) A novel glucokinase activator modulates pancreatic islet and hepatocyte function. Endocrinology 146:3696–3701
7. Futamura M, Hosaka H, Kadotani A et al (2006) An allosteric activator of glucokinase impairs the interaction of glucokinase and glucokinase regulatory protein and regulates glucose metabolism. J Biol Chem 281:37668–37674
8. Fyfe MC, White JR, Taylor A et al (2007) Glucokinase activator PSN-GK1 displays enhanced antihyperglycaemic and insulinotropic actions. Diabetologia 50:1277–1287
9. Coope GJ, Atkinson AM, Allott C et al (2006) Predictive blood glucose lowering efficacy by glucokinase activators in high fat fed female Zucker rats. Br J Pharmacol 149:328–335
10. Gorman T, Hope DC, Brownlie R et al (2008) Effect of high-fat diet on glucose homeostasis and gene expression in glucokinase knockout mice. Diabetes Obes Metab 10:885–897
11. Nakamura A, Terauchi Y, Ohyama S et al (2009) Impact of small molecule glucokinase activator on glucose metabolism, beta cell function and mass. Endocrinology 150:1147–1154
12. Nakamura A, Shimazaki H, Ohyama S, Eiki J, Terauchi Y (2011) Effect of long-term treatment with a small-molecule glucokinase activator on glucose metabolism, lipid profiles and hepatic function. J Diabetes Invest 2:276–279
13. Johnson D, Shepherd RM, Gill D, Gorman T, Smith DM, Dunne MJ (2007) Glucose-dependent modulation of insulin secretion and intracellular calcium ions by GKA50, a glucokinase activator. Diabetes 56:1694–1702
14. Wei P, Shi M, Barnum S, Cho H, Carlson T, Fraser JD (2009) Effects of glucokinase activators GKA50 and LY2121260 on proliferation and apoptosis in pancreatic INS-1 beta cells. Diabetologia 52:2142–2150
15. Withers DJ, Gutierrez JS, Towery H et al (1998) Disruption of IRS-2 causes type 2 diabetes in mice. Nature 391:900–904
16. Kubota N, Tobe K, Terauchi Y et al (2000) Disruption of insulin receptor substrate-2 causes type 2 diabetes due to liver insulin resistance and lack of compensatory beta-cell hyperplasia. Diabetes 49:1880–1889
17. Kubota N, Terauchi Y, Tobe K et al (2004) Insulin receptor substrate 2 plays a crucial role in beta cells and the hypothalamus. J Clin Invest 114:917–927
18. Matschinsky FM (2009) Assessing the potential of glucokinase activators in diabetes therapy. Nat Rev Drug Discov 8:399–416
19. Bonadonna RC, Heise T, Arbet-Engels C et al (2010) Piragliatin (RO4389620), a novel glucokinase activator, lowers plasma glucose both in the postabsorptive state and after a glucose challenge in patients with type 2 diabetes mellitus: a mechanistic study. J Clin Endocrinol Metab 95:5028–5036
20. Meininger GE, Scott R, Alba M et al (2011) Effects of MK-0941, a novel glucokinase activator, on glycemic control in insulin-treated patients with type 2 diabetes. Diabetes Care 34:2560–2566
21. Iino T, Hashimoto N, Sasaki K et al (2009) Structure-activity relationships of 3,5-disubstituted benzamides as glucokinase activators with potent in vivo efficacy. Bioorg Med Chem 17:3800–3809
22. Weir GC, Bonner-Weir S (2007) A dominant role for glucose in beta cell compensation of insulin resistance. J Clin Invest 117:81–83
23. Lingohr MK, Briaud I, Dickson LM et al (2006) Specific regulation of IRS-2 expression by glucose in rat primary pancreatic islet beta-cells. J Biol Chem 281:15884–15892
24. Maechler P, Jornot L, Wollheim CB (1999) Hydrogen peroxide alters mitochondrial activation and insulin secretion in pancreatic beta cells. J Biol Chem 274:27905–27913
25. Jhala US, Canettieri G, Screaton RA et al (2003) cAMP promotes pancreatic beta-cell survival via CREB-mediated induction of IRS2. Genes Dev 17:1575–1580
26. Ashcroft FM (2005) ATP-sensitive potassium channelopathies: focus on insulin secretion. J Clin Invest 115:2047–2058
27. Porat S, Weinberg-Corem N, Tornovsky-Babaey S et al (2011) Control of pancreatic beta cell regeneration by glucose metabolism. Cell Metab 13:440–449
28. Kushner JA, Ye J, Schubert M et al (2002) Pdx1 restores beta cell function in Irs2 knockout mice. J Clin Invest 109:1193–1201
29. Suzuki R, Tobe K, Terauchi Y et al (2003) Pdx1 expression in Irs2-deficient mouse beta-cells is regulated in a strain-dependent manner. J Biol Chem 278:43691–43698
30. Shih DQ, Heimesaat M, Kuwajima S, Stein R, Wright CV, Stoffel M (2002) Profound defects in pancreatic beta-cell function in mice